J Eng Math (2009) 63:213–239
DOI 10.1007/s10665-008-9232-4

The effects of nonsymmetry in a branching flow network

Nick Ovenden · Frank Smith · Guo Xiong Wu

Received: 27 June 2007 / Accepted: 8 April 2008 / Published online: 16 May 2008

Abstract A planar flow network consisting of successive generations of bifurcating vessels located downstream from a single mother vessel containing an incident fully developed flow is investigated. The theory and analysis developed which are for relatively thin vessels apply to small, medium or large networks. Although each successive bifurcation is in effect from a new mother vessel to two daughters, the networked system splits these into different types of bifurcation, the middle ones being inertial and the edge ones being viscous–inviscid in view of the wall conditions. The influences of network shapes, topology and end-pressure differences on the flow ahead of and inside the network are examined. Distinct local and global forms of upstream influence are active. The effects are especially marked in terms of non-symmetry, which leads to a global upstream influence, displaces the whole incident flow and particularly affects the motions near the outermost walls; there the non-symmetrical effects govern the induced wall shear stress and pressure and the solution dependence is very sensitive because of the realistic incident flow. Results from lattice-Boltzmann simulations are also described, and comparisons are then made with the theory and analysis. Pressure and shape control are considered in detail.

Keywords Branching · Flow networks · Lattice-Boltzmann techniques · Upstream influence

1 Introduction

Networks of branching vessels containing fluid flow play important roles in many applications, from plumbing and underground waterways to biomedical applications concerning physiology. The biomedical applications are in fact the ones of most interest for the present study. These include, in particular, models of part or even the whole of the human circulation, as well as the cerebral blood network, and on a more refined scale modelling of the Circle of Willis, arteriovenous malformations and multi-branching structures such as the Middle Cerebral Artery. See [1–7]. Our motivation then is from biomedical applications concerning networks of vessels.

Previous work on branching or networks includes many analytical, computational and experimental studies, such as those of [8–20]. Among these are numerous investigations of bifurcations with or without a few further

N. Ovenden (✉) · F. Smith
Department of Mathematics, University College London, Gower Street, London WC1E 6BT, UK
e-mail: nicko@math.ucl.ac.uk

G. X. Wu
Department of Mechanical Engineering, University College London, Torrington Place, London WC1E 7JE, UK

generations of bifurcations following on downstream. Many or most theoretical discussions, however, are on one- or two-dimensional models and assume some kind of flow symmetry at each branching junction or bifurcation, partly, if not entirely, for the sake of theoretical or similar progress and partly to claim application to three-dimensional branching flows. There are also many network studies of various sorts and styles including rational or irrational treatments. Few or no existing network analyses seem to allow for both inviscid and viscous effects except for [20]; yet both of these effects would seem relevant for the medium to large flow rates or Reynolds numbers that operate in many biomedical applications.

It is potentially very important also to examine the effects of flow non-symmetry, whether due directly to shape effects at a bifurcation or indirectly to lack of symmetry in the entire network, and to consider the corresponding bias that spreads throughout the network. Little effort appears to be reported on this aspect despite its obviously wider applicability. Other aspects including three-dimensional effects, abrupt one-to-many branching and successive generations of bifurcations are considered recently by [20] and [21], while further background work is by [2,4,11,22,23]. Our main concern in the present paper is with motion at medium to large Reynolds numbers in a network incorporating non-symmetry.

Key questions concern the mode or modes of upstream influence that act within a network, the interaction between local and global pressure requirements, the role of inertia compared with that of viscous forces, and indeed the interplay between inviscid and viscous behaviour. Given that lubrication theory as used in some approaches strictly assumes rather large length scales, much greater than the typical viscous lengths, and that an arteriovenous malformation and other distinguished networks are comparatively short, there is the issue of what happens for shortened networks. Questions arise also on how much progress can be made analytically, on whether any size of network can be handled theoretically, on describing analytically the influence of end-pressures and geometry or topology on a network, on how to match possibly very different types of flows and vessels present inside a network, and on whether theory works at realistic Reynolds numbers. How the flow ahead of the network is affected is also of concern, in terms of upstream shaping [16] and upstream influence [24], as well as mass flux. These issues are especially interesting for a non-symmetric network.

Concerning our specific interest, since the flow for a large network is very difficult to solve in full by direct computation, the present contribution starts with use of the theory of interaction involving an inviscid core and thin viscous wall layers, among several other features, to help improve physical understanding and to create predictions and comparisons. In fact, we use theory/analysis for Reynolds numbers Re large and then computations at medium Re, and compare them. The aim is to find the mass-flux–pressure relationship for the network, the induced pressures and shear stresses at the outermost walls where the flow is at its most sensitive and particularly the non-symmetric component of the entire motion, in addition to considering the effect of cutting out some vessels downstream. Complexities arise from the geometry, non-symmetry and vorticity due to the incident motion. The work highlights the short- and long-scale physical changes which are a common feature for the networks of various sizes that are studied: an example is sketched in Fig. 1. It is found that the core relations, the jump conditions in pressure and vorticity arising at almost every bifurcation and the wall-layer equations all play roles in the interactive flows present. The theory developed appears to be complete, viscous–inviscid and largely analytical. It not only explains how a relatively low pressure, for example in one daughter vessel, tends to draw fluid into that daughter, producing a displacement in the flow ahead and hence a non-symmetry, but also how such non-symmetry can arise from various other sources within the network. The theory takes the flow to be two-dimensional.

The investigation then is aimed at a large viscous–inviscid network; see Figs. 1 and 2. In terms of the entire system there are three types of unit to accommodate. The first unit comprises the very first bifurcation; there could be several first units in a system in practice but here we consider only a single one. *Wall-touching units* or *edge vessels* are the outermost vessels that share one wall with the mother vessel. *Internal units* or *core vessels* share no wall with the mother. So the type of a unit depends on whether at some normal y-location the incident internal velocity profile $u_0(y)$ in the stream-wise (axial) direction is zero or not within the unit: see Fig. 2. For a large network the internal units are generally the most common, in which $u_0(y)$ is nonzero everywhere. Wall-touching units which have $u_0(y)$ being zero at just one edge corresponding to one of the two outer walls are rarer in a general large network. The first unit is unique in that it has $u_0(y)$ zero at both of its edges as they are the outer walls. Each

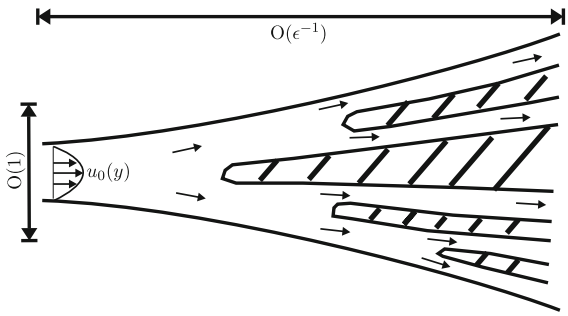

Fig. 1 Schematic diagram (not to scale) of the typical branching network containing successive bifurcations downstream of an original mother vessel, with a fully developed $u = u_0(y)$ incident motion. The axial length scale $\epsilon^{-1} = \delta^{-1/2}$. Non-symmetry is permitted

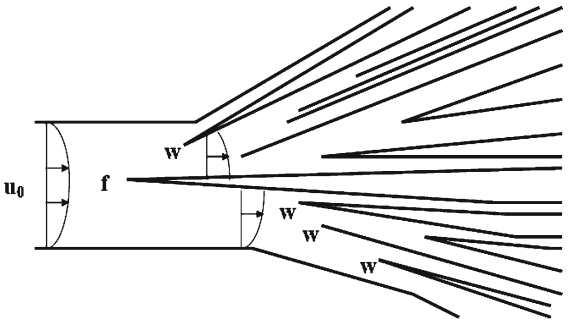

Fig. 2 Showing the different types of units present in a multiply-bifurcating system, in particular the first unit (denoted **f**), the wall touching ones (denoted **w**) and the internal ones (all others unlabelled). Typical parts of the velocity profile are as seen

unit in the network consists locally of one mother vessel M and two daughters D1, D2, and the whole network is an assembly of such units joined together through appropriate pressure and mass flux conditions.

There is distinct mechanics at work in the three different types of units. In the mother, as part of a first unit, the viscous wall layers on both outermost walls play vital roles in both ensuring no slip at the walls, and interacting with the core flows, leading to possible free interactions in accordance with existing literature. In the daughters, again as part of a first unit, the viscous roles are likewise vital in terms of the displacement being known, at least up to a constant, from the core flows. The viscous role of each daughter vessel also forms part of every wall-touching unit, in contest with the motion in other vessels, including all internal units, which is quasi-inviscid and only satisfies the tangential-flow condition along dividers or internal walls. This is in addition to the mechanics associated with the shorter-scale behaviour near the branch junctions, which manifests itself as localised jumps in pressure and velocity within the major axial length scale of interest.

For the sake of generality the network must be assumed to be non-symmetric as mentioned previously. The axial length scale involved in the first unit scales with the 1/7th power of the Reynolds number [24] and governs the non-symmetric upstream influence in the system apart from the global influence afforded by the end-pressure control. The length scale examined could be enlarged of course but a specifically non-symmetric upstream influence is absent over such lengths in general.

The flow features are addressed below in non-dimensional form with velocity field (u, v) in respective Cartesian coordinates (x in the broadly axial direction, y in the direction normal to that), pressure $p(x, y, t)$ and time t. In the usual manner, the relevant dimensional scalings are a typical flow speed U^*, a representative length L^* and the fluid density ρ. The Reynolds number $\mathrm{Re} = U^*L^*/\nu$, with ν denoting the kinematic viscosity, and as stated earlier planar motion is assumed. We define a stream function ψ in the usual manner by $u = \psi_y$ and $v = -\psi_x$ and use it where convenient in different parts of the analysis. For definiteness the incident mother vessel is taken to have a relatively long upstream portion, yielding incoming fully developed flow in the absence of bifurcations, although this is readily altered to accommodate a general incoming velocity profile. Separation is largely suppressed throughout.

We begin in Sect. 2 with the first bifurcation or what is in essence the fundamental system of a 1-to-2 bifurcation alone, while Sect. 3 builds on that to consider a 1-to-3 or 1-to-4 network, where new matching phenomena arise. Section 4 then extends this to a larger network, bringing in the responses for internal units in addition to those of the first unit which is that considered in Sect. 2 and the wall-touching units which are those introduced in Sect. 3. Effective solution jumps, for example in the induced pressure, enable matching to take place between different parts or units of networks. The theory assumes small spread angles, i.e., all walls are close to being aligned, and it also assumes sufficiently smooth divider and other wall shapes. In the work, nonlinear theory is set up first, followed by

linearized analysis. Lattice-Boltzman computations are described in Sects. 5 and 6 together with comparisons with the earlier analysis. Section 7 provides further discussion.

The following sections detail the relations between pressure difference and fluxes in the various vessels of the network, which are built up to satisfy the overall pressure differences imposed on the network. Flux is represented by a displacement function, conveniently, and the latter also gives the induced velocities in the vessels.

2 The first bifurcation

The first bifurcation is itself equivalent to a simple one-to-two network with prescribed end pressures as well as a first unit in a wider system. With the total pressure difference and hence the pressure gradient being imposed over the whole system, strictly we define U^* here as $U^* = L^{*2}G^*/(\rho\nu)$ where G^* is the pressure gradient imposed over a long length scale rather than a local pressure gradient, which may be significantly larger. Hence the Reynolds number Re, based on the typical tube width L^*, is $L^{*3}G^*/(\rho^*\nu^2)$.

The orders of magnitude of the different contributions in the Navier–Stokes equations (These equations, together with the overall pressure differences accross the network, and the given vessel-shape conditions, constitute the full problem to be addressed of course) then show that the longest axial viscous length scale is O(Re) provided that u, v and y are O(1) at most. The present study is of length scales somewhat shorter than that of the viscous length scale.

We describe modelling of a planar network of bifurcating tubes as in Fig. 1 starting at $x = 0$, the general case of a non-symmetric network being addressed. The quantities used now are non-dimensional, a typical axial speed induced in the incident mother flow and a typical tube width both being of order unity. The mother flow is taken to be fully developed motion with no slip at the walls, with stream-function profile $\psi_0(y)$ (so $u_0(y) = \mathrm{d}\psi_0/\mathrm{d}y$) but unknown total mass flux. Steady flow is assumed over a long length scale that is nevertheless short compared with the viscous length Re above, together with zero pressure far upstream in the mother and prescribed pressures at the downstream ends of the network.

Asymptotic expansions of the flow solutions in the various vessels are proposed here and in later setions and they are then substituted in the Navier–Stokes equations. The following sub-sections discuss in turn the viscous wall layers, the core of the motion, the interplay between the end pressures and possible local discontinuities induced in the flow over the present length scale, and representative flow solutions.

2.1 The viscous wall layers

The upstream-influence length scale axially is long, of $\mathrm{O}(\mathrm{Re}^{1/7})$, from [24]. Putting $\delta = \mathrm{Re}^{-2/7}$, which is small, we write $x = \delta^{-1/2}X$ with X of order unity. The thin viscous layer at the lower outer wall near $y = 0$ then has thickness of order δ from order-of-magnitude arguments. So $y = \delta(Y + S(X))$, say, and $S(X)$ denotes the scaled given lower-wall shape, with the flow solution expanding as

$$[u, \psi, p] = \left[\delta U, \delta^2\Psi, \delta^2 P(X)\right] + \cdots, \tag{1}$$

the typical mass flux thus being of $\mathrm{O}(\delta^2)$. The scaled wall pressure P is independent of Y because of the normal momentum balance. In consequence the nonlinear viscous wall-layer equations

$$U = \Psi_Y, \quad V = -\Psi_X, \tag{2a}$$

$$UU_X + VU_Y = -P_X(X) + U_{YY}, \tag{2b}$$

control the wall-layer behaviour in scaled terms. The boundary conditions required, for matching with the core flow and for no slip at the outer wall, are of the form.

$$U \sim \lambda_0\,(Y + A(X) + S(X)) \quad \text{as} \quad Y \to \infty, \tag{2c}$$

$$U = \Psi = 0 \quad \text{at} \quad Y = 0, \tag{2d}$$

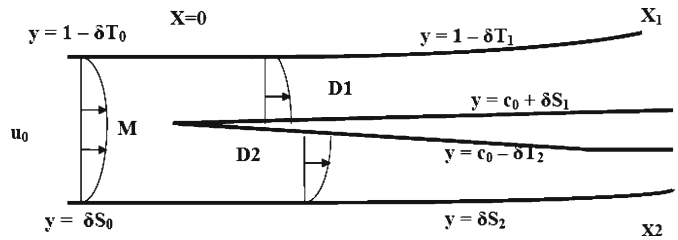

Fig. 3 The one-to-two branching flow or first unit studied in Sect. 2. The mother vessel is M, the daughters are D1 (upper) and D2 (lower) with a divider near $y = c_0$ as shown, and the wall shapes are represented by thicknesses δS_n and δT_n ($n = 0, 1, 2$) along $y = 0$, c_0 or 1. The pressure variations are of order δ^2 throughout. Here X is zero at the branch junction

where the O(1) positive constant λ_0 stands for the scaled incident wall shear and the function $A(X)$ is unknown. Apart from the issue of upstream influence, the negative boundary-layer displacement or inviscid slip velocity effect $A(X)$ can be obtained (to within a factor related to the mass flux) by the core-flow solution valid outside the wall layer, as shown in the next sub-section. In that case, the viscous wall-layer problem determines the δ^2-scaled lower-wall pressure response P to within a constant. In effect the function $A(X)$ plays the role of a displacement and a velocity as indicated in (2c), as well as a mass flux in (5) below.

Adjoining the upper wall $y = 1$ there is a similar layer in which $y = 1 - \delta\left(Y^+ + T(X)\right)$, where $T(X)$ denotes the scaled upper-wall shape measured, as is Y^+, in an inward direction. The expression (1) applies again but with $\psi - \psi_0(1)$ and with $u = \delta U^+ + \cdots$, and so on, while the governing equations and constraints are in effect as in (2a)–(2d) except for the requirement

$$U^+ \sim \lambda_0^+ \left(Y^+ - A(X) + T(X)\right) \quad \text{as} \quad Y^+ \to \infty, \tag{3}$$

which replaces (2c), the change in sign of the A term arising from the core displacement. Here the positive constant λ_0^+ denotes the scaled incident shear at the upper wall. The δ^2-scaled upper-wall pressure P^+ again is to be determined.

The controlling equations (2a–d) and (3) in both lower and upper wall layers form a nonlinear system together with a relation between $A(X)$ and $P(X)$, $P^+(X)$ or with $A(X)$ prescribed. If the disturbances produced by the network pressures and various wall thicknesses present are relatively small, however, then the system becomes linearized, as discussed later on in this section.

2.2 The core

Suppose here that we have a single 1-to-2 branching, then, as in Fig. 3, with mother M, upper daughter D1 and lower daughter D2. The mother vessel has walls situated at $y = 1 - \delta T_0(X)$, $y = \delta S_0(X)$, while those of D1 are at $y = 1 - \delta T_1(X)$, $y = c_0 + \delta S_1(X)$ and those of D2 are at $y = c_0 - \delta T_2(X)$ and $y = \delta S_2(X)$, where $\delta S_n(X)$, $\delta T_n(X)$ for subscript $n = 0, 1, 2$ are the wall or divider thickness contributions of O(δ); the subscripts $n = 0, 1, 2$ refer in turn to the thicknesses in the mother, upper daughter and the lower daughter vessels, respectively. The total divider thickness in the current case is $\delta\,(S_1(X) + T_2(X))$, and the divider is positioned astride the level $y = c_0$ with c_0 being an O(1) constant lying between zero and unity. Accordingly the shape $S(X)$ in (2c) is given by $S_0(X)$, $S_2(X)$ and, similarly, $T(X)$ in (3) is defined by $T_0(X)$, $T_1(X)$, for negative and positive X in turn.

The inviscid core within the upper daughter D1 acts mostly as if distinct from that in the lower daughter D2 and likewise for the viscous lower wall layer, over the present length scales. In the core of M, D1, D2 the pressure p is of O(δ^2), with the stream function ψ and p expanding respectively as

$$\psi = \begin{cases} \psi_0(y) + \delta\{A_0(X)u_0(y) + f_0(y)\} + \cdots, \text{ in M} \\ \psi_0(y) + \delta\{A_1(X)u_0(y) + f_1(y)\} + \cdots, \text{ in D1} \\ \psi_0(y) + \delta\{A_2(X)u_0(y) + f_2(y)\} + \cdots, \text{ in D2} \end{cases} \tag{4a}$$

$$p = \begin{cases} \delta^2 p_0(X, y) + \cdots, \text{ in M} \\ \delta^2 p_1(X, y) + \cdots, \text{ in D1} \\ \delta^2 p_2(X, y) + \cdots, \text{ in D2} \end{cases} \tag{4b}$$

$$f_n(y) = \Theta_n \psi_0(y) \quad \text{for} \quad n = 0, 1, 2, \text{respectively.} \tag{4c}$$

Here, $\psi_0(y) = \lambda_0\left(y^2/2 - y^3/3\right)$ and $u_0(y) = \lambda_0\left(y - y^2\right)$, corresponding to the fully developed Poiseuille flow in the absence of any bifurcation, whereas the constant Θ_n is an unknown associated with the mass flux alteration which is proportional to $f_n(y)$, is of order δ in the core and is included for completeness. More generally, $\psi_0(y)$ and $f_n(y)$ could be taken as arbitrary no-slip profiles in y but for definiteness we will keep to the fully developed forms. Also within (4) a pressure variation of size larger than that shown would be independent of y and unsupportable at the outer walls, as the subsequent explicit solutions verify. Further, it can be shown that the undeveloped viscous layers on the internal dividers of the daughters can be taken to have negligible impact on the flow, i.e., they are passive, implying a tangential-flow condition in D2 on the given divider underside $y = c_0 - \delta T_2(X)$. In terms of the linearisation used, the Blasius viscous thicknesses that grow on the divider are actually a fraction $\delta^{1/2}$ smaller than the original order δ for $X = \mathrm{O}(1)$, essentially adding only $1.7208(\delta X/u_0(c_0))^{1/2}$ to $S_1(X)$ and $T_2(X)$ for positive X. The typical Blasius thickness here agrees with the traditional estimate of $\mathrm{Re}^{-1/2}x^{1/2}$ given that x is of order $\mathrm{Re}^{1/7}$. The core flow thus yields the governing equations

$$\begin{aligned} &u = u_0 + \delta u_1 + \cdots, \\ &v = \delta^{3/2} v_1 + \cdots && \text{from continuity,} \\ &u_0 \partial u_1/\partial X + v_1 u_0' = 0 && \text{from the axial momentum balance} \\ &u_0 \partial v_1/\partial X = -\partial p_n/\partial y && \text{from the normal momentum balance.} \end{aligned}$$

Hence, the velocity correction u_1 is given by the $\mathrm{O}(\delta)$ term written in (4a) and v_1 by $-(\mathrm{d}A_n/\mathrm{d}X)u_0$, satisfying the continuity and axial-momentum equations, while the normal-momentum equation shows that $\partial p_n/\partial y = u_0 \mathrm{d}^2 A_n/\mathrm{d}X^2$, producing a significant normal pressure gradient. Taking $T_2(0)$ as zero without loss of generality thus yields the classical thin-channel result

$$A_2(X) = T_2(X) + K_2, \quad \text{for } X > 0 \tag{5}$$

(since $u_0(c_0) > 0$), which determines the function $A_2(X)$ to within the additive constant K_2. The pressure remains unknown in D2, and it is likewise unknown in D1 where the subscript 2 is replaced by 1 in the above working together with $-S_1(X)$ replacing $T_2(X)$; thus $A_1(X) = -S_1(X) + K_1$ for $X > 0$. The effective slip velocities $\delta\lambda_0 A(X)$ and $-\delta\lambda_0^+ A(X)$ at the outer edges of the inviscid core as $y \to 0, 1$ drive the viscous wall layers, which is where $S_{0,2}(X)$ and $T_{0,1}(X)$ first make their presences felt.

On the other hand, upstream influence is present in the mother tube M occupying $X < 0$, where the core has

$$p_n(X, y) = P(X) + \frac{\mathrm{d}^2 A_n}{\mathrm{d}X^2} \int_0^y u_0^2(s)\mathrm{d}s \tag{6}$$

with $n = 0$ and $P(X)$ being the scaled lower-wall pressure. The result (6) follows from the normal momentum balance. So, the upper wall pressure P^+ is related to the pressure at the lower wall P by

$$P^+(X) = P(X) + q\frac{\mathrm{d}^2 A_n}{\mathrm{d}X^2} \tag{7}$$

where the positive constant q is the integral in (6) evaluated at $y = 1$. Altogether, this yields a free-interaction behaviour [24] in which, for X large and negative, and with $\lambda_0 = \lambda^+ = \lambda$, say,

$$A_0(X) \sim K_0\, \mathrm{e}^{\kappa X}, \quad \text{where } \kappa = \lambda^{5/7}\left(-6\mathrm{Ai}'(0)/q\right)^{3/7}, \tag{8}$$

with Ai(x) being the Airy function. Here (8) represents an elliptic effect in the sense that the constant K_0 depends on the global flow behaviour downstream whereas the value of κ is fixed and for the incident fully developed motion

described earlier is 5.18767... for $\lambda = 1$. The slip effect $A(X)$ which helps to drive the two viscous wall-layer responses is identical to $A_0(X)$, $A_2(X)$ along the lower wall, for $X < 0$, $X > 0$ respectively, and $A_0(X)$, $A_1(X)$ along the upper wall.

The pressures within the two daughters are not given by the same relations (6) and (7), with $n = 1, 2$.

In the two daughters for $n = 1, 2$, by contrast, the displacements A_1, A_2 are known to within additive constants from (5) and also the presence of the divider astride $y = c_0$ allows the daughter pressures to be discontinuous there in the normal direction. So the relations (6) and (7) used to determine the pressure in the mother vessel no longer apply. Similar relations apply within the daughters but they act to fix the induced pressures on either side of the divider, thereby predicting the forces acting on the divider once the outer wall pressure is determined.

2.3 The end pressures and local jumps at branching junctions

The end pressures p at certain X-stations upstream or downstream in the vessels are specified in the sense that the scaled pressure values p_n and hence the wall pressure values

$$P\,(X_{-\infty}) = P^+\,(X_{-\infty}) = 0, \quad P^+(X_1) = P_1, \quad P(X_2) = P_2, \tag{9}$$

are imposed, i.e., the constants P_1 and P_2 are specified. The wall pressure conditions P^+ and P (or P^-) are here applied at general finite stations downstream within the daughter vessels in anticipation of a network developing from those stations, which would be further branch junctions requiring subsequent pressure matching there. See Sects. 3 and 4. Here the station $X_{-\infty}$ is sufficiently upstream of the branching, and indeed in the present setting is at minus infinity, while X_1, X_2 are downstream in the two daughters.

Based on the findings in [6,7,22], initially we might expect local pressure jumps also to be present at the branching junction, axially from 0− to 0+. The jumps would help accommodate the set pressures upstream and downstream in (9), with a local change in mass flux of

$$\delta u_0(c_0)\,[A_1(0+) - A_0(0-)]\,,$$

where $A_1(0+)$, $A_2(0+)$ are equal, and at first sight there seems nothing to doubt their presence here. Such abrupt jumps are believed (hypothesized) to be absent in the current first-unit setting, however, essentially due to the free interaction in (8) which operates instead and yields a longer upstream effect. Nowhere else within the current bifurcation or within the larger networks studied subsequently is there such a free interaction. Moreover the free interaction is able to accommodate a wide range of set pressure differences through a linear response with $\mathrm{e}^{\kappa X}$ alone or a nonlinear response with extra $\mathrm{e}^{2\kappa X}$ terms etc. as in [24]. This is in line also with the absence here of any means to support pressures of $\mathrm{O}(\delta)$, while the likelihood of significant separation being induced in the lower or upper viscous wall layer if the abrupt local change in displacement is positive or negative, by contrast with Sects. 3 and 4 below, is another although lesser factor. Hence, the scaled pressures and displacement effects here are taken as continuous across $X = 0$. This leaves the constants $K_{0,1,2}$ equal and the displacement and slip $A(X)$ continuous at the origin, implying that there is no abrupt change in mass flux there.

In consequence, the end pressures P_1, P_2 are forced to be functionally related, as in the examples of the next sub-section. This end-pressure relation is consistent with the longer-scale pressure behaviour. Another consequence from the absence of pressure variations and jumps of order δ concerns the mean flow alterations in (4), namely the $f_n(y)$ which must all be equal in the current bifurcation, so that

$$f_1(y) = f_2(y) = f_0(y) = f(y), \tag{10}$$

say. Thus there is little change in the mass flux and vorticity due to the current pressure differences. For a 1-to-2 network alone the $f_n(y)$ can further be equated to zero without loss of generality, whereas if the current bifurcation is just the first bifurcation in a larger system then the common value of the profiles $f_n(y)$ above remains unknown at this stage. We set $f(y)/u_0(y) = g(y)$ for convenience.

2.4 Flow solutions

For small effective displacements $\hat{c}(X)$, which represents $(A(X) + S(X))$ in (2c) and $(-A(X) + T(X))$ in (3), a linearized form applies instead of (2a–2b) as mentioned earlier. The quantities $U - \lambda_0 Y$ $(= \hat{u}$ say), the pressure and so on are all small then, and by taking a Fourier transform in X defined for a function $g(X)$ as

$$g^f(\omega) = \int_{-\infty}^{\infty} g(X)\, \mathrm{e}^{-\mathrm{i}\omega X}\, \mathrm{d}X,$$

the following lower-wall properties are obtained

$$\hat{\tau}^f(\omega) = \frac{\partial \hat{u}}{\partial Y}\Big|_{Y=0} = 3\mathrm{Ai}(0)(\mathrm{i}\omega\lambda)^{1/3}\lambda\hat{c}^f(\omega), \quad \hat{p}^f(\omega) = \alpha(\mathrm{i}\omega)^{-1/3}\hat{c}^f(\omega). \tag{11}$$

Here, we take again λ_0, λ_0^+ equal to λ for convenience, while $\hat{\tau}$ is the wall shear perturbation at the lower wall, and the constant $\alpha = 3\mathrm{Ai}'(0)\lambda^{5/3}$ is negative. An exactly analogous solution holds in the upper layer.

Ahead of the branching, (11) and its upper-wall analogue are coupled through the relation implied by (7), formally

$$P^{+f}(\omega) = P^f(\omega) - q\omega^2 A^f(\omega) \tag{12}$$

and so the formal solution for the displacement is

$$A^f(\omega) = \alpha\frac{\left(S^f(X) - T^f(X)\right)}{(q(\mathrm{i}\omega)^{7/3} - 2\alpha)}. \tag{13}$$

The pole arising in (13), where the denominator vanishes, is responsible directly for the upstream influence, in which $A(X)$ takes the form in (8) for all $X < 0$ if the shape effects $S(X)$, $T(X)$ or more generally the nonsymmetric part of $S(X) - T(X)$ is zero in $X < 0$. However, Eq. (7) does not hold in $X > 0$. Therefore (12) and (13) apply only for a half-range sense. The references [25] and [26] used that feature to apply a Wiener–Hopf technique for the solution. Here we use a different approach as it is more readily applicable to larger networks.

After the branching, $X > 0$ and the second expression in (11) gives the wall-pressure transform solution directly with $\hat{c}(X)$ replaced by $(A(X) + S(X))$ along the lower wall and by $(-A(X) + T(X))$ along the upper wall. Thus, on inversion we have

$$P = \frac{\alpha}{\Gamma(1/3)}\int_{-\infty}^{X} [A(s) + S(s)]\,(X - s)^{-2/3}\mathrm{d}s, \tag{14a}$$

$$P^+ = \frac{\alpha}{\Gamma(1/3)}\int_{-\infty}^{X} [-A(s) + T(s)]\,(X - s)^{-2/3}\mathrm{d}s, \tag{14b}$$

while formally from the first expression in (11) the wall shear stress perturbation is predicted by the finite-part result

$$\hat{\tau}(X) = -\sqrt{3}\mathrm{Ai}(0)\lambda^{4/3}\frac{\alpha}{2\pi}\int_{-\infty}^{X} [A(s) + S(s)]\,(X - s)^{-4/3}\mathrm{d}s \tag{14c}$$

at the lower wall and similarly at the upper wall.

A particular case of interest is that of negligible wall-shape effects ($S = T = 0$ throughout) but with the flow being driven by differences in the end pressures or by various divider placements, i.e., c_0. Then $A(X) = K_0\,\mathrm{e}^{\kappa X}$ in M, $A(X)$ is some constant K_1 in D1, and $A(X)$ is K_2 in D2. On the other hand, continuity across $X = 0$ requires $K_0 = K_1 = K_2$. Hence,

$$A(X) = \begin{cases} K_0\,\mathrm{e}^{\kappa X} & \text{in M} \\ K_0 & \text{in D1} \\ K_0 & \text{in D2.} \end{cases} \tag{15}$$

From (14a,b) the wall pressure solutions are therefore

$$P(X) = -P^+(X) = \begin{cases} \alpha\kappa^{-1/3}K_0\,\mathrm{e}^{\kappa X} & \text{for } X < 0, \\ 3\dfrac{\alpha}{\Gamma(1/3)}\kappa K_0\,\mathrm{e}^{\kappa X}\int_{-\infty}^{X} u^{1/3}\,\mathrm{e}^{-\kappa u}\,\mathrm{d}u & \text{for } X > 0. \end{cases} \tag{16}$$

The results agree with those of [26] after a technical error is corrected in the latter work, incidentally. The end conditions then require the second and third constraints of (9) to hold. So, as anticipated, the end pressures over the present length scale are inter-related. Indeed, if the end stations X_1, X_2 are equal, then P_1, P_2 are forced to be equal but opposite in value as seen in [7]. It is interesting also that the solution above appears to be independent of the divider positioning c_0.

Solution properties for the pressure-driven and a variety of shape-driven cases are presented in Fig. 4(a–c). In every case the downstream pressure is imposed as $-1/3$ with $\kappa X_1 = 4$. The presence of induced upstream influence in exponential form is clear throughout, with Fig. 4(a, b) showing the effective shape-and-displacement function $\hat{c}(X)$, the scaled pressure and the wall-shear-stress perturbation induced at an outer wall when the only shape effects acting are in the daughters as represented by the parameter b_1. The three cases given in Fig. 4(a) in particular highlight the shaping effect in provoking quite distinct behaviour ahead of the bifurcation. The controlling influence of the downstream pressure value is also clear in the case of $b_1 = 0$ in the sense that a sign reversal of pressure simply changes the sign of the entire flow result upstream. The solutions presented also include upstream shaping effects in Fig. 4(c), where the upstream wall shaping is proportional to the parameter C_1. The results altogether indicate that in general a rise and then fall in $\hat{c}(X)$ make the pressure P fall (favourable pressure gradient) and then rise (adverse), and vice versa, as is physically sensible. In Fig. 4(b) for instance the pressure response upstream produces an adverse pressure gradient, giving a very pronounced axial decrease in wall shear stress along with the displacement $-A(X)$ increasing, meaning that the effective outer slip $A(X)$ for the lower-wall layer is decreasing. The results also indicate that the displacement ahead of the branch junction can be an upward or downward trend depending on the vessel shapes as well as the downstream pressures and this dependence is quite a sensitive one. A contraction in the width of any vessel involved broadly leads to a favourable pressure gradient and increasing wall shear locally, and expansion to an adverse pressure gradient with decreasing wall shear, as expected, but the global upstream influence and the end pressures can accentuate or counteract those trends.

To summarize the results of Sect. 2, the pressure-driven case leads to the result (15) for the induced displacement function which also gives the effect on mass flux. The mechanism of upstream influence is clear in terms of the exponential contribution in (15) showing the influence on the motion in the mother vessel. The displacement (15) acts to determine the induced pressure via the response in the viscous outer-wall layers, yielding (16), while the outer-wall shear stress perturbations stem from (14c). The shear stress on the thin divider here and in the other networks throughout the paper is given by the classical Blasius form and is much larger than the outer-wall shear stresses. The shape-driven cases follow a similar pattern based on the flow solutions in (11)–(14c) above.

3 The second or third bifurcation

To enlarge the system to incorporate a further bifurcation next, we may suppose that there is a 1-to-3 or -4 network, exactly as in the network of Sect. 2 but succeeded by at least one wall-touching unit. The notation is such that it allows generalisation, taking account of necessary relabelling from daughter to granddaughter vessel and so on; see Fig. 5. Then an extra feature appears in the following.

3.1 The core surrounding the next junction

Again attention can be restricted initially to a lower part, consisting now of a daughter flow (for $d2 < y < d1$ with $d2$ being zero and $d1 < 1$) described essentially as in (4), (5) and two granddaughters for $d2 < y < d0$ and $d0 < y < d1$ which begin at $X = X_0 > 0$. These as a unit can be regarded anew as a mother M and daughters D1, D2. The lower of these granddaughters has a motion also described essentially by (4), (5). The upper one, however, which is vessel D1 now, must usually suffer higher typical pressure variations of $O(\delta)$ such that in its core

$$\psi = \psi_0(y) + \delta\psi_{n^*} + \cdots , \tag{17a}$$

where

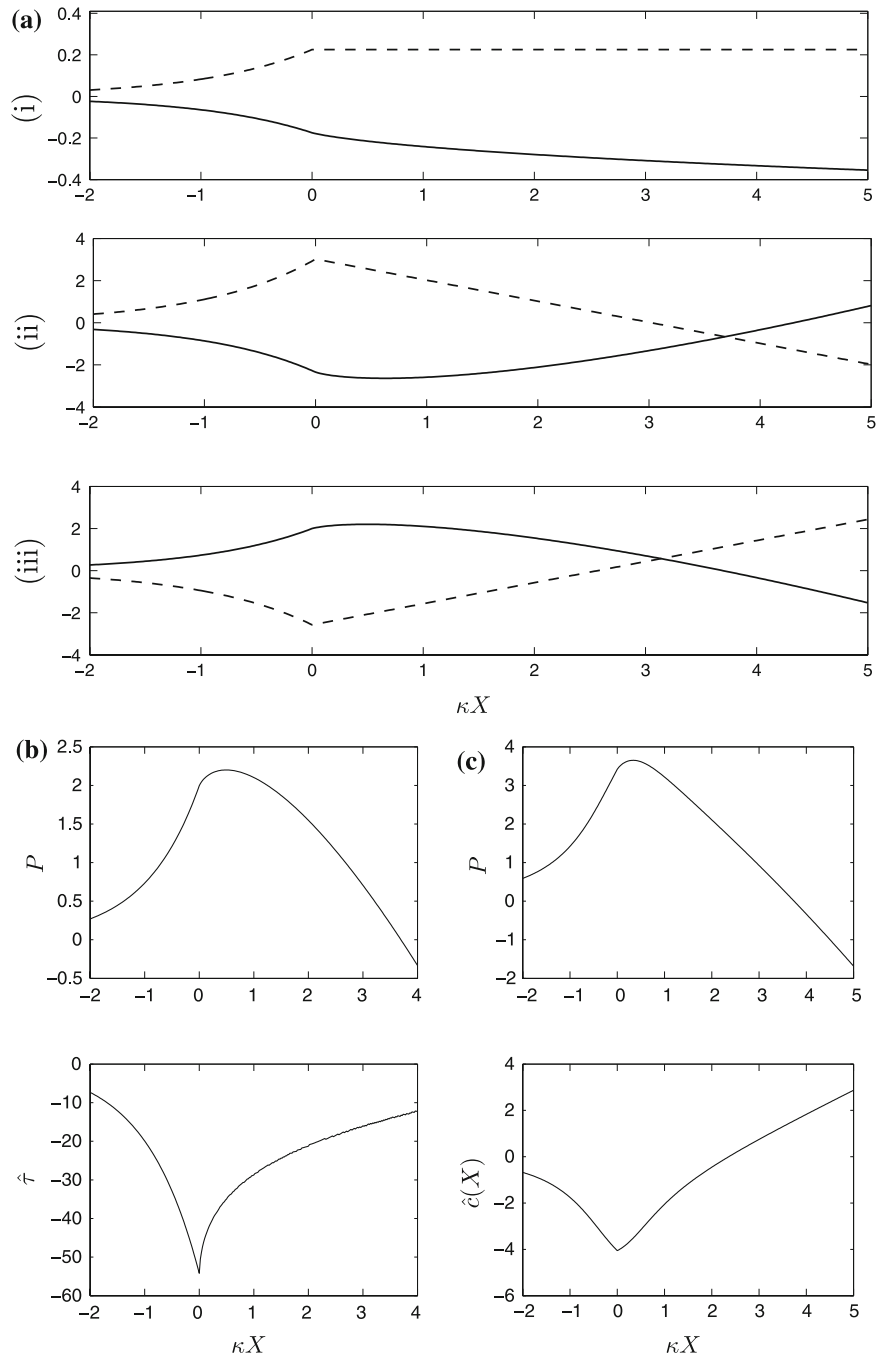

Fig. 4 One-to-two bifurcating flows for wall shapes such that $S_1 = C_1/(1+C_2X^2)$ in the mother for $X < 0$ and the daughter gap-width factor S_2+T_2 is b_1X in $X > 0$. (**a**) For $C_1 = 0$, lower-wall pressure $P(\kappa X)$ (solid lines) and $\hat{c}(\kappa X)$ (dashed lines) for the pressure-driven case of (i) $b_1 = 0$ and the shape-driven cases (ii) $b_1 = -1$ and (iii) $b_1 = +1$. (**b**) Wall-shear-stress perturbation and pressure for the shape driven case where $b_1 = 1$, again for $C_1 = 0$. (**c**) As (a) but for the upstream shape-driven case where $b_1 = 1$ but $C_1 = -2$, $C_2 = \kappa^2$

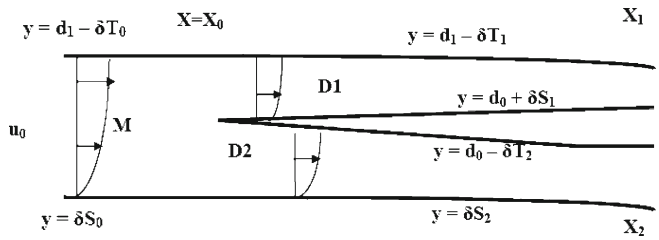

Fig. 5 For a one-to-three or one-to-four system as addressed in Sect. 3, this shows a typical wall-touching unit. Locally, the mother vessel is M, the daughters are D1 and D2, but the incident velocity profile $u_0(y)$ is positive except at $y = 0$. The wall shapes are given by the thicknesses δS_n and δT_n $(n = 0, 1, 2)$ along $y = d_2,\ d_0,\ d_1$ as seen from bottom to top. Here $d_2 = 0$, while $X = X_0$ at the bifurcation. The pressure variations are of $O(\delta^2)$ within M and D2, but of $O(\delta)$ within D1

$$\begin{aligned} &\psi_n = \{D_n(X, y) + g_n(y)\}\, u_0(y), \\ &p = \delta p_{n*} + \cdots, \quad \text{with } n = 1. \end{aligned} \tag{17b}$$

where $d_0 - \delta T_2(X)$ and $d_0 + \delta S_1(X)$ are now the underside and topside, respectively, of the divider between these two granddaughters. The additional flux profile $g_1(y)u_0(y) = f_1(y)$ is arbitrary at this stage but $g_1(d_0)$ is zero without loss of generality. From substitution in the Navier–Stokes equations and from the tangential flow condition at the topside $y = d_0+$, we have

$$D_1(X, y) = -p_{1*}(X) \int_{d_0}^{y} u_0^{-2}(s)\mathrm{d}s - S_1(X) + \gamma_1, \tag{18}$$

compare with (4), (5) and (6). Here $\psi = \psi_0(d_0) + \delta\gamma_1 u_0(d_0)$ is constant along the topside of the divider, i.e., the lower wall of vessel 1 here, to two orders of working. The δ-scaled pressure p^* which is independent of y and the flux constant γ_1 are unknown. The tangential flow condition at the opposite side or upper wall $d_1 - \delta T_1(X)$ of this vessel requires ψ constant, $\psi_0(d_1) + \delta\,(\Gamma_1 + g_1(d_1))\, u_0(d_1)$ say, requiring $D_1(X, d_1)$ to equal $T_1 + \Gamma_1$ for some unknown constant Γ_1, where d_1 and Γ_1 can be identified with the quantities c_0 and $K_0 + g(c_0) - g_1(c_0)$, respectively, in Sect. 2. Hence, with σ_1 standing for $\gamma_1 - \Gamma_1$, the result

$$p_{1*}(X) \int_{d_0}^{d_1} u_0^{-2}(y)\mathrm{d}y = \sigma_1 - \{S_1(X) + T_1(X)\}, \tag{19}$$

provides the pressure–thickness relationship within this vessel. The dependence on the axial change in scaled-gap thickness through the factor $S_1 + T_1$ is noted and contrasts with the nonsymmetric contribution $S - T$ in (13) holding upstream of the first bifurcation studied in the previous section. The inviscid thin-layer property (19) makes good physical sense as a decreasing gap width forces the axial velocity to increase to conserve mass and so the pressure must decrease in view of the momentum balance. Again axial continuity concerning g_1 is considered in the next sub-section. Finally here the viscous layers on the dividers are stronger than those on the outer walls in the sense that the former have typical inertial and viscous forces of order unity, while the typical forces within the outer wall layers are significantly smaller, making the outer layers more sensitive, and this aspect accounts for the tangential flow requirements being relevant as used in (17)–(19).

The extra feature of jumps usually occurring in the flow solution must now be accommodated.

3.2 The local jumps at the branching junction

The new solution jumps act (over the present length scale) in the pressure across the entrance of each of the granddaughters from X_0- to X_0+, given that u_0 is nonzero at the inner divider wall astride d_0 as well as d_1. The active jumps here are smoothed out on a shorter axial scale by an O(1) Euler region in $X - X_0$, similar to those encountered analytically and numerically in the [22] study and yielding overall another type of ellipticity through that region in which the linearised Euler equations hold as inertial forces dominate there.

Given that the local dynamics are predominantly inviscid it is desirable to follow a streamline from just upstream to just downstream of the typical jump region, first from vessel 0 (daughter) to vessel 1 (upper granddaughter). The corresponding change δy^* in the y position is described by

$$y^* = \frac{(\psi_{0*} - \psi_{1*})}{u_0} \quad \text{at any } y, \tag{20}$$

where the right-hand terms are evaluated at X_0- or X_0+ as appropriate, ψ_{1*} being the function in (17a) which applies for $X > X_0$ and ψ_{0*} being the $O(\delta)$ contribution in (4) with A now given by $T_0 + \Gamma_0$ for $X < X_0$; the constant Γ_0 identifies with K_2 in (5) and T_0 here is the old T_2 of Sect. 2. Conservation of the pressure head, the Bernoulli quantity $p + u^2/2$, along the streamline is then found to require that

$$u_0 u_{0*} + p_{0*} = u_0 u_{1*} + p_{1*} + (\psi_{0*} - \psi_{1*})\, u_0'(y), \tag{21}$$

again for all $d_0 < y < d_1$. Here $u_{1*} = \frac{\partial \psi_{1*}}{\partial y}$ while p_{1*} is given by (17b) but from the previous section u_{0*} is simply $(T_0 + \Gamma_0)u_0' + f_0'(y)$ and p_{0*} is identically zero. Substitution in (21) and further manipulation in which the pressure effects cancel out therefore yields

$$g_1(y) = g_0(y) - B_1, \tag{22}$$

relating g_1 back to g_0 and hence to g. In addition the constant B_1 can be seen to be $g_0(d_0)$ in this vessel. The main point, however, is that the pressure jump is admissible, as the incident velocity is nonzero at all y heights of that upper granddaughter, allowing the Bernoulli property to be maintained along each streamline without a large separation taking place. Overall mass conservation for the same daughter–granddaughter combination also leads to the result

$$(T_0(X_0) + \Gamma_0) = -p_{1*}\,(X_0+) \int_{d_0}^{d_1} u_0^{-2} \mathrm{d}y + \gamma_1 - B_1, \tag{23}$$

from (18) and Sect. 2, along with $\Gamma_1 = \Gamma_0 + B_1$.

Similarly a solution jump is admissible from vessel 0 to vessel 2, the lower granddaughter, although of a different form. It imposes a condition on the δ^2-scaled wall pressures near $y = 0$ just ahead of and behind the jump, namely

$$\left[P_0 + \lambda^2 A_0^2/2\right](X_0-) = \left[P_2 + \lambda^2 A_2^2/2\right](X_0+), \tag{24}$$

while keeping ψ_{2*} as $A_2 u_0(y) + f(y)$, given that $g_2 = g$. Mass conservation is automatically satisfied here. The avoidance of mass loss on the other hand relative to vessel 1 at the divider astride d_0 imposes the constraint

$$\gamma_1 = \Gamma_2 + g_0(d_0), \tag{25}$$

where A is $T_2(X) + \Gamma_2$ in the lower granddaughter. The constraint (25) follows from making use of (17) and (18) in the combined mass conservation with the upper granddaughter.

Also useful here is the relation (19) evaluated at X_0+ which gives

$$p_{1*}(X_0+) \int_{d_0}^{d_1} u_0^{-2} \mathrm{d}y = \sigma_1 - T_1(X_0) \tag{26}$$

since $S_1 = 0$ at X_0, and finally the scaled downstream pressure in

$$p_{1*}\,(X_1-) \int_{d_0}^{d_1} u_0^{-2} \mathrm{d}y = \sigma_1 - \{S_1\,(X_1-) + T_1\,(X_1-)\} \tag{27}$$

which is regarded as imposed at a prescribed X_1 station with $X_1 > X_0$.

In general the end pressures and flux constant Γ_0 help control the flow solution in a wall-touching unit through (23)–(28), for given vessel shapes. Thus A_0 is given by $T_0 + \Gamma_0$, while the end pressure condition (27) determines the scaled mass flux σ_1 in the particular vessel of concern, following which the junction pressure $p_{1*}(X_0+)$ is determined by (26). So γ_1 stems from (23) and then Γ_2 from (25), which yields the solution $A_2 = T_2 + \Gamma_2$. This determination of Γ_2 allows the analysis to move on to a next wall-touching unit if there is one downstream. With

A_0, A_2 being found as has just been described the wall-layer solution gives us P_0 and then P_2, taking account of the jump in (24), a jump which is negligible in the linearized case. Broadly, the influence of the downstream pressures holding inside the innermost vessels spreads upstream via the inviscid thin-layer property (19) whereas the outermost downstream pressures (and outer wall shapes S_0, S_2) have effect through the viscous wall-layer response.

The extra feature that an axial jump in displacement can occur across a granddaughter entrance from X_0- to X_0+ is caused by the presence of at least one inner vessel (an inner granddaughter) that does not share any containing wall with the mother vessel. The jump thereby becomes achievable and relevant, as a contrast to the setting in the previous section where one of the containing walls is always shared. In fact, the means to support higher pressures, of $O(\delta)$, than before exists simply because of the distinct geometry here compared with that considered in the previous section. The reason we feel that a jump is not called for at the first bifurcation is predominantly due to a free interaction operating instead and producing a longer scale effect there, and only there, as we mentioned. It might also be argued that one or other of the lower and upper walls would then be subjected to an adverse pressure gradient in the downstream portion of its Euler region and this would cause a different large-scale separated flow structure to apply; thus if $A_1(0+) > A_0(0-)$ the abrupt local acceleration of the lower-wall layer would be acceptable within the overall model but the corresponding deceleration of the upper wall layer not, and similarly if $A_1(0+) < A_0(0-)$. It is a moot point, but in any case no abrupt change in local mass flux occurs at the first bifurcation.

The present solution jump at the second or third bifurcation, accompanied by a change in vorticity as in (22) across the daughter entrance GD_1 but not across GD_2, also helps to accommodate the set pressures upstream and downstream which are imposed in similar fashion to those in (9) for the mother and each of the three or four downstream vessels here [7,22]. At the outer walls in particular, where the incident velocity is close to zero, the viscous layers of (1)–(3) allow the Bernoulli quantity $p + u^2/2$, scaled as $P + U^2/2$, to be conserved as required along each local inviscid streamline by means of a scaled pressure jump. This jump in the case of small thicknesses is $\lambda^2(\Gamma_0^2 - \Gamma_2^2)/2$, from (24), and in keeping with the analysis in Sect. 2.4 as discussed below. The local wall-layer behaviour is in essence that described further in [22]. Strictly all the jumps here are subject to the restriction that at the lower (upper) wall A ($-A$) should increase abruptly to provide a favourable effect.

3.3 The repercussions

Extending the above, in the 1-to-4 case as in Fig. 5 similar considerations apply to an upper part say, comprising a daughter flow and two granddaughters which begin at another station $X = X_0 > 0$. The discontinuities on the X scale associated with the pressure jumps are smoothed out over a shorter axial scale by an Euler region of length $O(1)$ in x as studied in [7,22,23] and mentioned earlier. The Euler region provides a direct communication between the two granddaughters and the daughter immediately ahead.

The property of the pressure and displacement being in general discontinuous across $X = X_0$, or the flux constants Γ_0, Γ_2 being unequal, permits adjustment of the constants in order to allow the inner granddaughter pressure to satisfy any downstream pressure condition of the form in (9) or (19). A like property holds for the upper daughter D1 by means of flux constants there.

A linearized analysis now yields merely small discontinuities in displacement and hence in pressure. As a result of the above it is found that a jump is also induced in the effective $A(X)$ function here which although still similar to (5)ff now generally has

$$A(X) = \begin{cases} K_2\, \mathrm{e}^{\kappa X}, \\ T_0(X) + K_2, \\ \text{(discontinuity)}, \\ T_2(X) + \Gamma_2. \end{cases} \tag{28}$$

The result (28) refers to mother, daughter and granddaughter vessels, unlike (15), which is for a mother and two daughters. We recall that $K_2 = \Gamma_0$. The discontinuous form (28) now drives the viscous wall-layer response by means of the constraint (2c). The displacement constants K_2, Γ_2 in (28) are controlled not only by the outermost

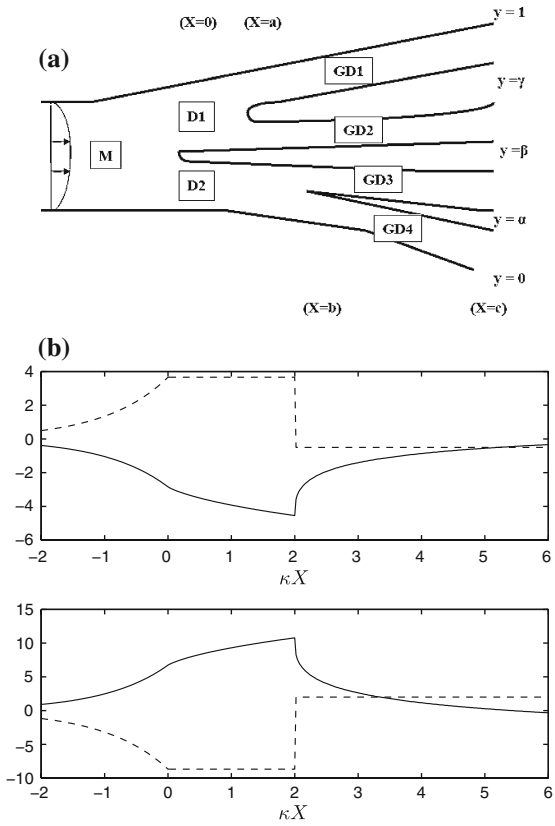

Fig. 6 (**a**) A specific one-to-four network comprising M, D1, D2 and grandaughter GD1 to GD4 from top to bottom as shown. Bifurcations are at $X = 0,\ a,\ b$, the downstream ends are all at $X = c$, and the motion is subject to end pressure differences $\delta^2\pi_1, \delta\pi_2, \delta\pi_3, \delta^2\pi_4$ from top to bottom. (**b**) Two solution examples with negligible thickness effects, giving $\hat{c}$ (dotted lines), P (solid lines) and opposite signed Γ_0 values illustrating quite different non-symmetrical responses upstream

(lower granddaughter) imposed pressure downstream but also by the inner (upper) granddaughter pressure imposed downstream.

For the specific 1-to-4 network sketched in Fig. 6(a) there are two wall-touching units and one first unit. If wall shaping can be neglected the network is *pressure-driven* by downstream pressures $\delta^2\pi_1$, $\delta\pi_2$, $\delta\pi_3$ and $\delta^2\pi_4$ imposed at the station $X = c$ in granddaughters GD_1, GD_2, GD_3, GD_4, as shown, while the dividers start at $(X, y) = (0, \beta)$ (M bifurcating to D_1, D_2), (a, γ) (D1 to GD1, GD2) (b, α) (D2 to GD3, GD4). Here $0 < a < b < c$ and $0 < \alpha < \beta < \gamma < 1$. Wall-shape effects are negligible. The wall-touching unit that comprises D2, GD3, GD4 yields from (26) and (27) $\sigma_1 = \pi_3 I_3$ and a junction pressure $p_{1*}(X_0+)$ in GD3 equal to π_3 where I_3 is the integral in (27) with limits (α, β). Hence this unit has its $\gamma_1 = \Gamma_0 + \sigma_1 + g_0(d_0)$ and its $\Gamma_2 = \gamma_1 - g_0(d_0)$, leaving A_0 as Γ_0 but A_2 as $\Gamma_0 + \sigma_1$. The lower-wall layer consequently is driven by

$$A(X) = \begin{cases} \Gamma_0\, e^{\kappa X} & \text{for } X < 0 \\ \Gamma_0 & \text{for } 0 < X < b \\ \Gamma_0 + \pi_3 I_3 & \text{for } b < X < c \end{cases} \tag{29}$$

The lower-wall pressure P is then given by (14a) with $S = 0$, and so the condition $P(c) = \pi_4$ fixes the flux constant Γ_0. Similar reasoning applies to the wall-touching unit that consists of D1, GD1, GD2 and, accordingly, the upper wall layer sees

$$A(X) = \begin{cases} \Gamma_0\, e^{\kappa X} & \text{for } X < 0 \\ \Gamma_0 & \text{for } 0 < X < a \\ \Gamma_0 + \pi_2 I_2 & \text{for } a < X < c \end{cases} \tag{30}$$

in contrast with (29) and, of course, is driven by $-A(X)$ rather than $A(X)$. Here I_2 is the integral in (27) with limits (β, γ). The incident profile alteration $g(y)$ is seen to have no influence on (29) and (30) despite the induced vorticity

jumps. The pressure $P^+(X)$ follows from (14b) with $T = 0$, and then the requirement $P^+(c) = \pi_1$ confirms that (as in the previous section) the outermost downstream pressures must be related. The formula (14c) gives the outer wall shear stress distributions.

For the corresponding *shape-driven* case suppose the gap-width reductions downstream are δh_1, δh_2, δh_3 and $\delta^2 h_4$ in GD1 − 4, again from top to bottom, where each h stands for $S + T$. The negative displacement acting at the lower wall is then

$$A(X) = \begin{cases} \Gamma_0\, \mathrm{e}^{\kappa X} & \text{for } X < 0 \\ T_2(X) + \Gamma_0 & \text{for } 0 < X < b \\ T_4(X) + \Gamma_0 - H_3 + h_3 & \text{for } b < X < c \end{cases} \tag{31}$$

and a similar form applies at the upper wall. Here $H_3 = S_3(b) + T_3(b)$ is the gap-width reduction at the entrance to the vessel GD3 and, as $T_3(b) = 0$ at the bifurcation, then $H_3 = S_3(b)$. The steps leading to the expressions in (31) follow directly from the argument associated with (28). The jump in $A(X)$ at the station $X = b$ is again apparent. The wall-layer properties are then given by (14a–c). Clearly the two parts of the network that are generated on either side of the very first divider can be treated separately, both here and in larger networks.

The solutions in Fig. 6(b) are for the pressure-driven case and show the scaled pressure induced at an outer wall for the specific 1-to-4 network of Fig. 6(a) with negligible wall thickness effects. Clearly for a 1-to-3 system the number of branching junctions as seen from an outermost wall is 1 or 2, whereas for a 1-to-4 system the number can be 1, 2 or 3 and an internal unit as in the following section might be produced. Larger networks to which we shall come soon can involve not only more branching junctions as seen from an outermost wall but also more branching junctions unseen from that wall, as in Fig. 1, for example. In the current results again a contraction of an outer tube width say broadly leads to a favourable pressure gradient and increasing wall shear there but the discontinuities due to the branching junctions along with upstream influence and end pressures can provoke an opposite effect. The combined behaviour affects the non-symmetry substantially, as the results here illustrate, switching the incident flow from side to side through the displacement effect rather than altering the total mass flux.

In summary, Sect. 3 has shown that for a pressure-driven small network leading to three or four granddaughter vessels the effects on the induced displacement A (and hence mass flux) at the outermost walls have the form (29) at the lower wall and (30) at the upper wall. Thus, after the exponential upstream influence in the mother each daughter flow has an interval in which A is constant, then a jump in A at the second branching (to two granddaughters), and then downstream another interval of constant A. Given such a displacement the outermost wall pressures and shear stresses respond according to the results in (14a–c). The corresponding flow in the granddaughters is given by (17)–(19) subject to the jumps in the solution explained in Sect. 3.2. For a shape-driven small network (31) holds and similar comments and interpretations apply.

4 More generations and a general network

To accommodate a third, fourth or any later bifurcation here, we suppose a network extending from 1 to more than 4 vessels, say a 1-to-N network. Again, we first consider its lower part, bearing in mind that the inner walls of the network are capable of sustaining pressures higher than those typical at the outer walls.

4.1 The core, and the local jumps at junctions

Yet another new feature enters as the new generation of vessels implied in such a network must contain some inner bifurcations which have nonzero incident velocity throughout. These lead to the so-called internal units, which provoke the higher $\mathrm{O}(\delta)$ pressures and corresponding solution jumps all the way across in y as well as for long distances axially upstream and downstream, while outermost bifurcations continue the earlier established trends of the wall-touching units and the first unit.

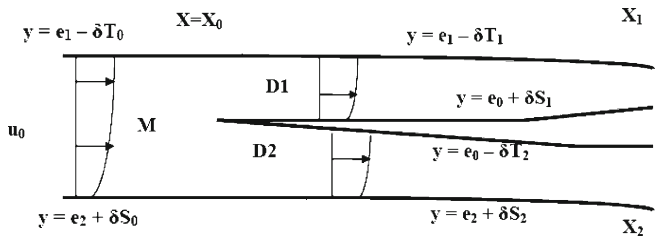

Fig. 7 The representative internal unit inside a larger network, studied in Sect. 4; here the incident velocity profile $u_0(y)$ is positive (non-zero) throughout. The local mother is M, while the daughters are D1, D2 as shown. Again the wall shapes are given by thicknesses δS_n and δT_n for $n = 0,\ 1,\ 2$ along $y = e_2$ (lower wall), $y = e_0$ (the divider) and $y = e_1$ (upper wall). Also X is labelled X_0 at the bifurcation and X_1 and X_2 at the downstream ends of D1 and D2, respectively. The pressure variations are of O(δ) throughout

For an internal unit, locally M, D1, D2 say as drawn in Fig. 7, the expressions in (17)–(19) apply exactly albeit with d_n replaced by constants e_n now where $0 < e_n < 1$, for $n = 0, 1, 2$. The functions $g_n(y)$ in (17a) for each vessel now are unequal in general, with $g_0(e_2)$, $g_1(e_0)$, $g_2(e_2)$ being zero, while

$$D_n(X, y) = -p_{n*}(X) \int_{e_B}^{y} u_0^{-2}(s)\mathrm{d}s - S_n(X) + \gamma_n, \tag{32}$$

where e_B denotes the minimum (lower wall) y-value inside each vessel. Furthermore the jump analysis in (20)–(23) remains valid but with the new feature that it now applies to the motion from M to both of the D1, D2 vessels.

The solution procedure for given end pressures $p_{n*}(X_n-)$ with $n = 1, 2$ in D1, D2 is as follows, for each internal unit. The flux constants σ_n are fixed individually by (27) and then the two junction pressures $p_{n*}(X_0+)$ by (26), suitably modified for the current unit. So next the flux $\gamma_0 - \Gamma_0$ in M stems from $\sigma_1 + \sigma_2$ as vorticity effects cancel. Note that here, the flux balances require $\Gamma_1 = \Gamma_0 + g_0(e_0)$, $\gamma_2 = \gamma_0$ and $\Gamma_2 = \gamma_1 - g_0(e_0)$. Thus, the relation

$$p_{0*}(X_0-)I_0 - p_{1*}(X_0+)I_1 = (\gamma_0 - \Gamma_0) - \sigma_1 - S_0(X_0), \tag{33}$$

obtained by making use of (32), serves to determine the junction pressure $p_{0*}(X_0-)$ in M. The pressure throughout the upstream part M of the unit is then given by the counterpart of (19), again using the relation (32), in the form

$$p_{n*}(X)I_n = \sigma_n - \{S_n(X) + T_n(X)\}, \tag{34}$$

with $n = 0$. The term I_n here is the integral of $u_0^{-2}(y)$ in y right across the vessel as in the previous section. The determination of the pressure in M in particular allows the analysis to move on to the next internal unit if there is one upstream.

As in Sect. 3, vorticity-correction effects adjust at each bifurcation, such that here g_0, g_1 and g_2 are given by $g(y) - g(e_B)$, and likewise onward into subsequent generations. They do not affect the main laws dictating pressure, however.

4.2 Solutions

The outer wall layers respond to the effective displacement or slip velocity $A(X)$ or $-A(X)$ produced by the core as mentioned earlier. To determine the influence of all the internal units present in a large network on that slip velocity requires tracking upstream from the most downstream internal unit and then fitting the most upstream unit thereby reached into the pattern of the wall-touching units of the previous section.

The prime example again is the *pressure-driven* case, but for the general setting of N final-generation vessels now. We suppose that the imposed pressures downstream are $\delta^2\pi_1$, $\delta\pi_2$, …, $\delta\pi_{N-1}$, $\delta^2\pi_N$ from top to bottom, and that the first bifurcation at $X = 0$ corresponds to the δ-scaled pressures (π_{N_1-1}, π_{N_1}) on either side of the divider, the first wall-touching unit to (π_{N_2-1}, π_{N_2}) with a bifurcation at $X = b_1$, the second wall-touching unit to (π_{N_3-1}, π_{N_3}) with a bifurcation at $X = b_2$, and so on until the last (π_{N-2}, π_{N-1}) with a bifurcation at $X = b_m$

say. Here N_1 and so on lie between 3 and $N-1$. All the internal units are further inside the network of course. The lower-wall flow is therefore controlled by the slip

$$A(X) = \begin{cases} \Gamma_0\, \mathrm{e}^{\kappa X} & \text{for } X < 0, \\ \Gamma_0 & \text{for } 0 < X < b_1, \\ \Gamma_0 + \sum_{j=N_1}^{N_2-1} \pi_j I_j & \text{for } b_1 < X < b_2, \\ \Gamma_0 + \sum_{j=N_1}^{N_3-1} \pi_j I_j & \text{for } b_2 < X < b_3, \\ \cdots & \\ \Gamma_0 + \sum_{j=N_1}^{N-1} \pi_j I_j & \text{for } b_{m-1} < X < b_m, \end{cases} \tag{35}$$

from (33), (34) applied to the network along with (29). Each I_j is the integral of $u_0^{-2}(y)$ across the final-generation vessel with end pressure π_j. The multiple jumps or discontinuities in $A(X)$ at the X-stations b_1 to b_m are clear, indicating the importance of the relative positioning of the branch junctions as well as the individual vessel thicknesses and pressures downstream. A similar formula holds at the upper wall. The ensuing outer-wall pressures and shear stresses may then be deduced as in (14), it being apparent that near the lower wall $S+A$ rather than some $S-T$ acts as an effective gap-width factor in the outermost vessel there and similarly $T-A$ acts near the upper wall.

The second specific example is the *shape-driven* case. We take the gap-width reductions downstream to be $\delta h_1, \delta h_2, \ldots, \delta h_{N-1}, \delta^2 h_N$ from top to bottom, and the first bifurcation at $X=0$ has gap-widths (h_{N_1-1}, h_{N_1}) downstream on either side of the divider, the first wall-touching unit has (h_{N_2-1}, h_{N_2}) with a bifurcation at $X=b_1$, the second wall-touching unit has (h_{N_3-1}, h_{N_3}) with a bifurcation at $X=b_2$, and so on until the last (h_{N-1}, h_N) with a bifurcation at $X=b_m$ say. The negative displacement for the lower-wall viscous flow is then

$$A(X) = \begin{cases} \Gamma_0\, \mathrm{e}^{\kappa X} & \text{for } X < 0, \\ T_2(X) + \Gamma_0 & \text{for } 0 < X < b_1, \\ T_4(X) + \Gamma_0 - H_1 + \sum_{j=N_1}^{N_2-1} h_j & \text{for } b_1 < X < b_2, \\ T_6(X) + \Gamma_0 - H_1 - H_2 + \sum_{N_1}^{N_3-1} h_j & \text{for } b_2 < X < b_3, \\ \cdots & \\ T_{2m}(X) + \Gamma_0 - \sum_{i=1}^{m-1} H_i + \sum_{j=N_1}^{N} h_j & \text{for } b_{m-1} < X < b_m, \end{cases} \tag{36}$$

where H_1 is now the gap-width reduction at the wall-touching unit from which all the vessels with subscript N_1 to N_2-1 emanate downstream, and so on across the network. The functions $T_2(X)$ and so on again give the successive divider shapes. A similar form holds for the upper wall. The multiple jumps or discontinuities in $A(X)$ at the X-stations b_1 to b_m are again apparent, re-indicating the importance of the relative positioning of the branch junctions but also now certain vessel gap-widths and their changes downstream. The summations in (36) show how different sections of the total downstream area affect the displacement throughout, coupled with the vessel areas at the wall-touching units. An expansion of total vessel area over the generations is seen to provoke a reduction in the A-effect at each step.

Results are presented in Figs. 8(a–d) and 9. These show the induced outer wall pressures P and the displacement-shape combinations C in Figs. 8(a–d) for several different cases of larger networks, along with an example in Fig. 9(a, b) of the inner-vessel pressures that can develop ahead of given downstream end-pressure distributions. Figure 8(a–c) has five bifurcations as seen from the outer wall while Fig. 8(d) is for ten. In each of the cases in Fig. 8(c, d) the network provokes a substantial upstream response with Γ_0 having a large magnitude, as do the P and C responses. The jump effects at each active wall-touching bifurcation then appear relatively small. In Figs. 9(a, b) the end pressures are set in the vessels marked 1–8 and those in the other vessels associated with that section of the network, i.e., 9–15, are unknown at the start. As expected physically, negative end-pressures tend to suck fluid away from the outermost walls towards the middle vessels, generating positive displacement, and vice versa for positive end-pressures. The inner pressures provoked are of greater magnitude than those at the outer walls, of course, but generally decrease with increasing distance away from the downstream distribution as seen in the cases of Fig. 9(a, b) because of the integral effect I_j, which represents an inertial response wherein the no-slip incident

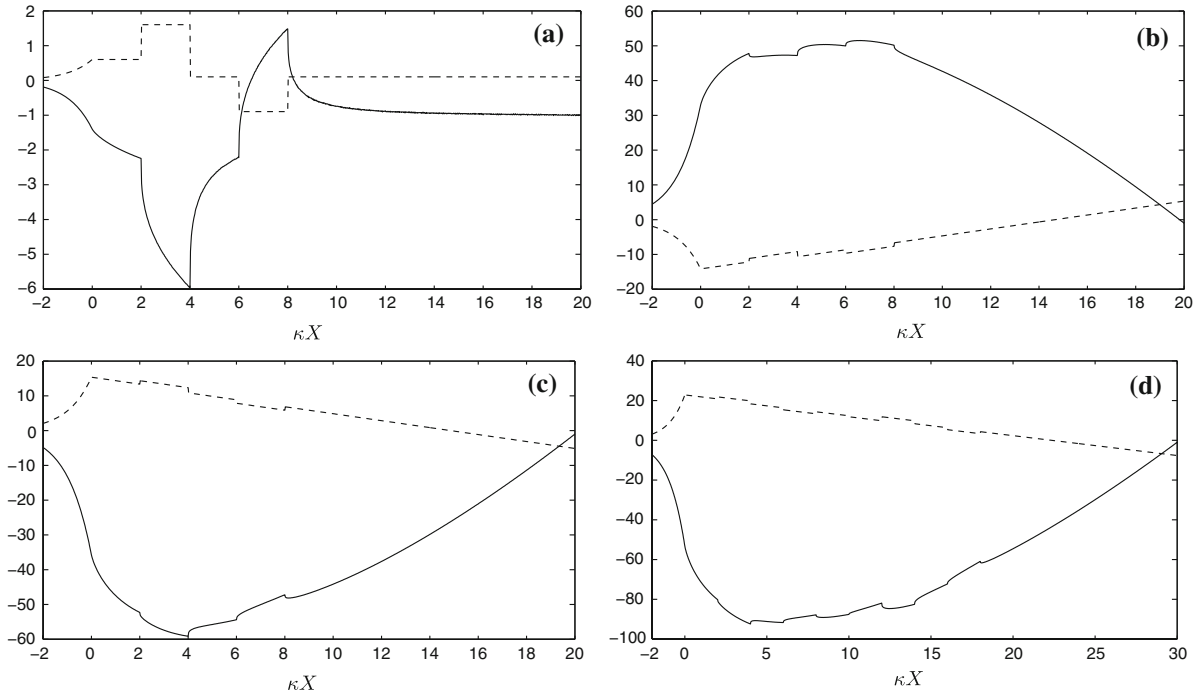

Fig. 8 Properties of larger networks. Solutions shown are for P (solid lines) and C (dashed lines) for four specific cases. The successive wall-touching gap-width factors $S+T$ here are $a_n + b_n X$ within the appropriate intervals of X. (**a–c**) Solutions for 5 bifurcations as seen at the outer wall. Here $b_{1-5} = 0$ in (**a**), $b_{1-5} = 1$ in (**b**) and $b_{1-5} = -1$ in (**c**), while $a_{1-5} = 0,\ 2,\ 0.5, -0.5,\ 0.5$ apart from the additional Γ_0 factor throughout, and the end station is at $\kappa X = 20$. (**d**) As (**a**) but with 10 bifurcations as seen from the outer wall; $b_{1-10} = -1$; $a_{1-10} = 0,\ 2,\ 0.5, -0.5,\ 0.5,\ 0,\ 2,\ 0.5, -0.5,\ 0.5$ except for Γ_0; the end station is at $\kappa X = 30$

velocity profile plays a significant role; it is also exactly in keeping with the scalings described at the start of this section. On the other hand (35) shows that the I_j integral effect can produce an exaggerated influence from the outermost vessels downstream since those vessels have u_0 being relatively small, implying in the limit an over-riding effect if one such vessel is especially close to the outer wall.

Certain other limiting cases are also worth mentioning here. Large values of N corresponding to many generations in the network make each sectional contribution to A in (35) approach the novel vertically integrated form

$$\int_{y_B}^{y_T} \hat{\pi}(y)\hat{\rho}(y)u_0^{-2}(y)\mathrm{d}y \tag{37}$$

Here $\hat{\pi}(y)$ is the imposed end-pressure distribution, while the effective density function $\hat{\rho}(y)$ denotes the relative width of the end vessels in the vertical y-direction, with y increasing from y_B to y_T in the particular section. The trend towards (37) can be seen in the results of Fig. 9(b). Comparatively rapid successive bifurcations tend to reduce the differences between $X = b_1$, $X = b_2$ and so on, drawing the branch junctions together horizontally. This mostly makes the expression for the slip $A(X)$ jump straight from the value Γ_0 in (35) to its final form

$$\Gamma_0 + \sum_{j=N_1}^{N-1} \pi_j I_j, \quad \text{for } X > b_1, \tag{38}$$

implying that all the end-pressure values then play a role sooner in the spatial sense. The configuration then models abrupt multiple branching of the kind studied by [7] but with allowance here for the important effects of nonsymmetry. Again the results in the figures indicate a tendency towards (38) applying if the spatial frequency of the bifurcations is enhanced.

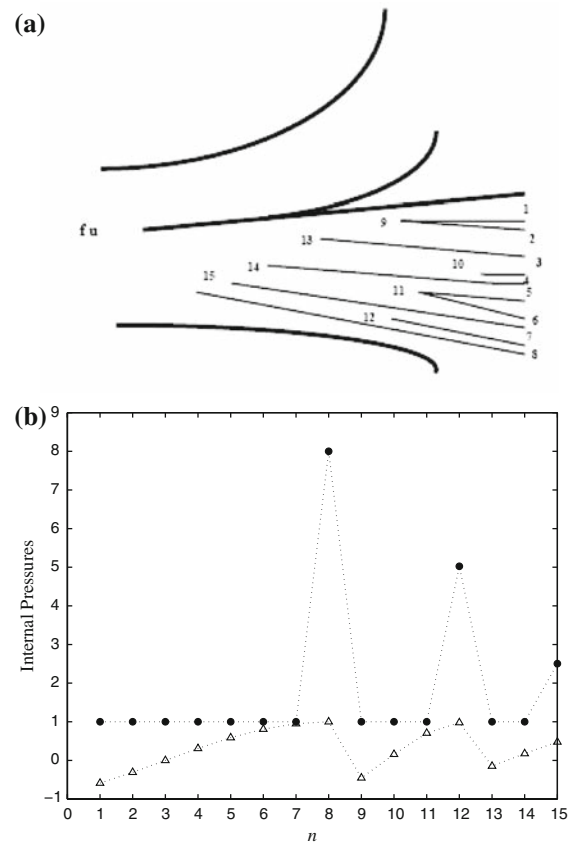

Fig. 9 Properties of larger networks. The successive wall-touching gap-width factors $S + T$ here are $a_n + b_n X$ within the appropriate intervals of X. For $a_n = 0$, $b_n = 0$ a specific pressure-driven network is shown in (**a**) and the development of the pressures in its internal vessels 1–15 is presented in (**b**) for two particular scaled end-pressure distributions as indicated: Case 1 (solid circles) has $1, \ldots, 1, 8$ and Case 2 (triangles) has $\sin(2\pi y)$ where the y-range is from 0.2 to 0.6

The summary of the main results of Sect. 4 is again expressed most clearly perhaps in terms of the pressure-driven case first. There the positive or negative displacement produced near the outer walls has the form (35) comprising exponential upstream influence in the mother vessel followed by intervals of uniform displacement between the successive branch junctions. The magnitude and the sign of the discontinuity at each junction depend on the pressures imposed downstream and on integral properties of the incident velocity profile as shown in (35). The effect on outer-wall pressures and shear stresses is then given by (14). Second, the shape-driven network invokes a similar response in (36). The results (32)–(34) apply to all of the more internal vessels of the core.

5 Comparison with direct simulations using lattice-Boltzmann techniques

In this section, we present some results obtained using lattice-Boltzmann methods to validate the analytical theory developed thus far in the paper. In recent years, lattice-Boltzmann methods have demonstrated themselves to be an accurate and useful numerical method for simulating fluid flows through and around complex geometries. No details of the lattice-Boltzmann method are provided here, but there is a wide literature on the techniques [27–29]. Here, an exactly incompressible lattice-Boltzmann equation scheme is used [30] with the BGK approximation for the collision operator [31]. No slip conditions at the wall are imposed using a standard bounce-back approach [29] and pressure conditions to drive the flow are imposed as in [32].

5.1 Comparison of a 1-into-2 branching

The geometrical setup for the first comparison consists of a straight channel with a divider that thickens downstream, leading to a fall in overall cross-sectional area from the mother vessel to the daughter vessels. Setting the channel to

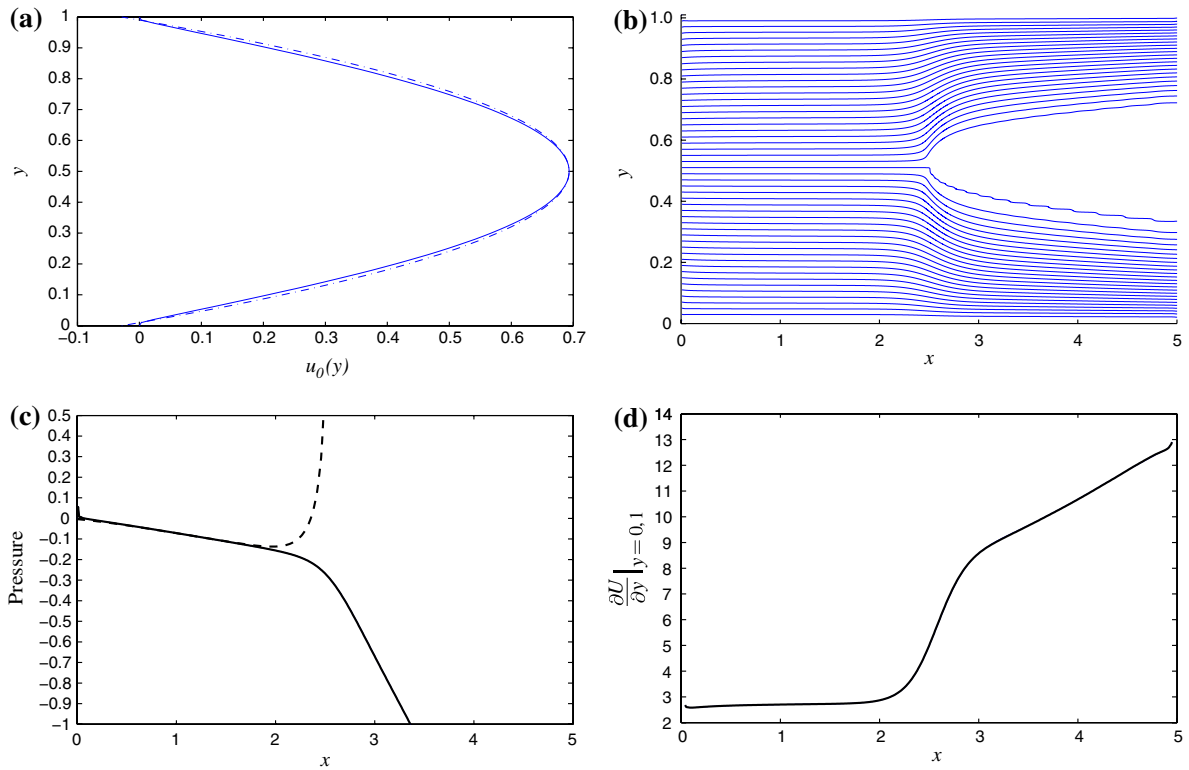

Fig. 10 Lattice-Boltzmann Simulation with 1-into-2 testcase with symmetric end daughter pressures. (**a**) Nondimensional inlet profile $u(x = 0) = u_0(y)$ (solid) versus Poiseuille (dotted). (**b**) Streamlines from LBM computation. (**c**) Nondimensional pressure at outer walls (solid) versus pressure on the midline $y = 0.5$ (dotted). (**d**) Nondimensional wall shear stress $\frac{\partial U}{\partial y}$ at the outer walls

have a length 5 times that of the width of the mother, the nondimensional fluid domain lies in the range $0 \leqslant x \leqslant 5$ and $0 \leqslant y \leqslant 1$ with the outer walls of the channel at $y = 0, 1$. The divider occupies the region

$$(y - 1/2)^2 < \frac{x - 2.5}{100} \quad \text{for } x \geqslant 2.5. \tag{39}$$

and a plot of the non-dimensionalised geometry is given in Fig. 10. Within a lattice-Boltzmann framework, this geometry is modelled as a regular lattice of 501×101 nodes with the top and bottom row of nodes representing no-slip solid boundaries. The divider shape given by (39) is also represented by non-fluid (solid) nodes. Note that computations have also been attempted on other sized lattices to ensure that the solutions presented are fully grid independent.

Fluid flow in the lattice-Boltzmann simulation is induced by fixing pressure drops between the upstream entrance to the mother tube at $x = 0$ and the downstream ends of the daughter tubes at $x = 5$. An iterative collision and streaming process is then repeated many times until the flow field converges to a steady state. During the iteration, the Reynolds number $\mathrm{Re} = U^* L^* / \nu$ is calculated based on the maximum axial velocity $U^* = \max u(x, y)$ attained in the flow field, with L^* as the width of the mother channel and ν as the internal kinematic viscosity of the lattice-Boltzmann model. This Reynolds number is gradually tuned during the iterations by altering the viscosity ν to obtain a steady state solution with $\mathrm{Re} = 200$.

Figure 10(a–d) presents some results for a symmetric case where the imposed pressure drops at the downstream end of both daughters are equal. Figure 10(a) shows the inlet profile generated by the lattice-Boltzmann simulation in comparison to a Poiseuille profile with the same mass flux. A plot of the streamlines obtained in the computation can be seen in Fig. 10(b), and Fig. 10(c) shows a plot of the pressures on the lower and upper walls $y = 0, 1$ and the midline pressure on the line $y = 0.5$. Lastly, Fig. 10(d) plots the upper and lower wall shears $\frac{\partial u}{\partial y}$ at $y = 0$ and $y = 1$.

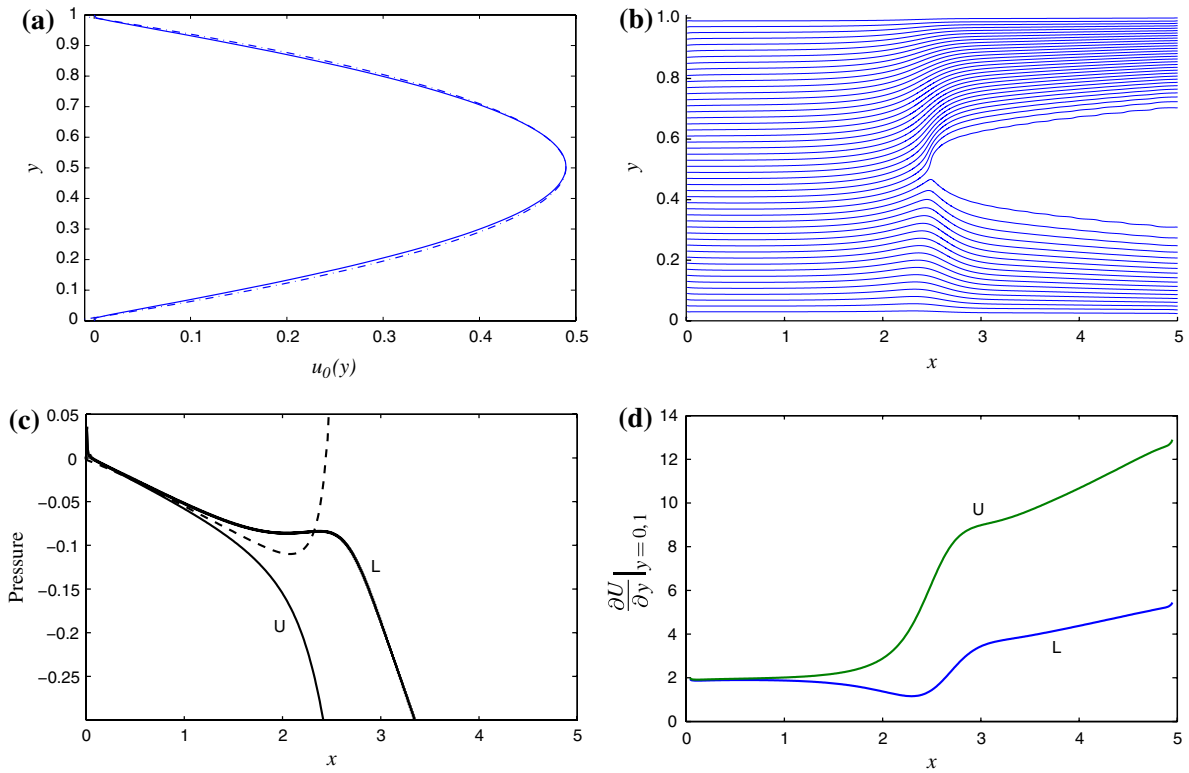

Fig. 11 Lattice-Boltzmann Simulation with 1-into-2 testcase with asymmetric end daughter pressures. (**a**) Nondimensional inlet profile $u(x = 0) = u_0(y)$ (solid) versus a Poiseuille profile (dotted). (**b**) Streamlines from the LBM computation. (**c**) Nondimensional pressure at the lower wall (L) and upper wall (U) and on the midline $y = 0.5$ (dotted). (**d**) Nondimensional wall shear stress $\frac{\partial U}{\partial y}$ at the lower wall (L) and upper wall (U)

Notice that there appears to be a degree of upstream influence extending an O(1) distance ahead of the divider, which raises the pressure in the centre of the channel and diverts the flow into the upper and lower daughters. As the daughter channels narrow downstream, the wall shear increases sharply and so does the pressure gradient needed to drive the flow through them.

Compare now the results for an asymmetric case in Fig. 11(a–d) where the pressure drops imposed at the downstream ends of both daughters are now unequal. For the case presented, the pressure drop in the upper daughter is three times that of the pressure drop in the lower daughter, although the Reynolds number remains at 200 as in the symmetric case. Observe how the asymmetry in the downstream pressures influences the flow much further upstream, indeed perceptively further than the O(1) distance apparent in the symmetric case above. The significant difference in the pressure drops in the upper and lower daughters naturally diverts a larger portion of the flow into the upper daughter, leading to a slowing of flow along the lower wall and an adverse pressure gradient there. This leads to a drop in the wall shear stress along the lower wall just ahead of the divider. Further downstream however, the lower wall shear stress quickly recovers to become increasingly attached as the divider thickens. And as one expects, strongly attached flow is observed along the entire upper wall particularly in the downstream segment within the daughter vessel.

We can compare the upstream influence observed in the lattice-Boltzmann simulation to that predicted by the analytical theory of [24], where the upstream pressure difference between the lower and upper walls of the channel is given by (7) and (8). Taking the log of the pressure difference predicted by the asymptotic theory implies that far upstream, for $x \ll 2.5$,

$$\log\big[p(x, y = 0) - p(x, y = 1)\big] = \kappa \mathrm{Re}^{-1/7} x + \text{constant} \tag{40}$$

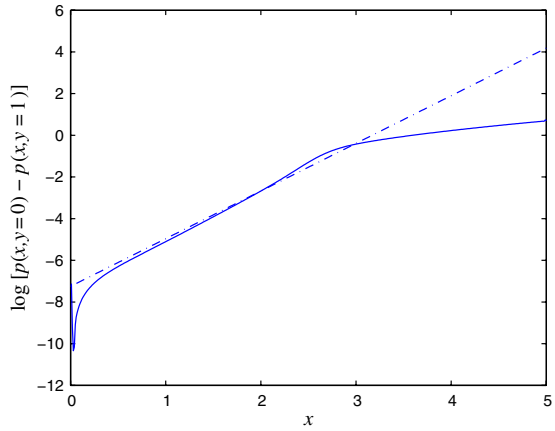

Fig. 12 LBM 1-into-2 case: Comparison of the log of the pressure difference between upper and lower walls obtained from the lattice-Boltzmann simulation (solid line) against our analytical theory which predicts a line of slope $\kappa \mathrm{Re}^{-1/7}$ (dotted line) upstream of the divider

The free-interaction parameter κ in this expression depends on certain properties of the incident velocity profile $u_0(y)$ [24]; explicitly it is given by

$$\kappa = \lambda_0^{5/7} \left(-\frac{6\mathrm{Ai}'(0)}{q} \right)^{3/7}, \tag{41}$$

where $\lambda_0 = u_0'(0)$ and

$$q = \int_0^1 u_0^2(y)\mathrm{d}y$$

have been defined earlier. For the asymmetric case, these values are calculated from the lattice-Boltzmann solution to be $\lambda_0 = 1.96$ and $q = 0.1223$. A straight line of the form (40), with a slope determined from these values, is plotted against the log of pressure difference obtained by the simulation in Fig. 12. Note that there is encouraging agreement between the asymptotic theory and computation over the majority of the flowfield upstream of the divider despite the theory being valid only in the limit $x \to -\infty$. The discrepancy around $x = 0$ can be explained by the finite extent of the computational domain and must occur due to the imposed pressure condition that $p(0, 0) = p(0, 1)$ in the computation. Close to the divider, the asymptotic expression becomes invalid and the flow pattern alters slightly as other upstream inviscid mechanisms acting on a shorter scale come into play.

6 Comparison of a 1-into-2-into-4 branching

The second geometrical set-up for the lattice-Boltzmann simulation is a network of vessels branching from one mother into two daughters, and then into four smaller vessels further downstream; see Fig. 13(a). The nondimensional computational domain is $0 \leqslant x \leqslant 6$ and $0 \leqslant y \leqslant 1$ with no-slip conditions at the outer walls at $y = 0$ and $y = 1$ respectively. A central divider occupies the following region

$$\left(y - \frac{1}{2} \right)^2 < \min \left(\frac{(x-3)}{100}, \frac{3}{200} \right) \quad \text{for } x \geqslant 3,$$

and two further straight thin dividers extend downstream from $x = 5$ and $x = 4.5$ in the upper and lower daughter, respectively. As a result the channel is ultimately split into four vessels of widths (from top to bottom) 0.20, 0.15, 0.18 and 0.16.

Fixed pressure boundary conditions are imposed upstream at $x = 0$ and downstream at the ends of the four smaller vessels (at $x = 6$) to induce a flow, with the viscosity ν tuned once again during the iterative cycle to obtain a target Reynolds number of 200. For the case shown, the nondimensional pressure is set to $p = 0$ at $x = 0$ in the mother and, at $x = 6$, the imposed nondimensional end pressures in each vessel are set, in order from top to bottom, to the values -0.75, -7.5, -3.0, -0.75.

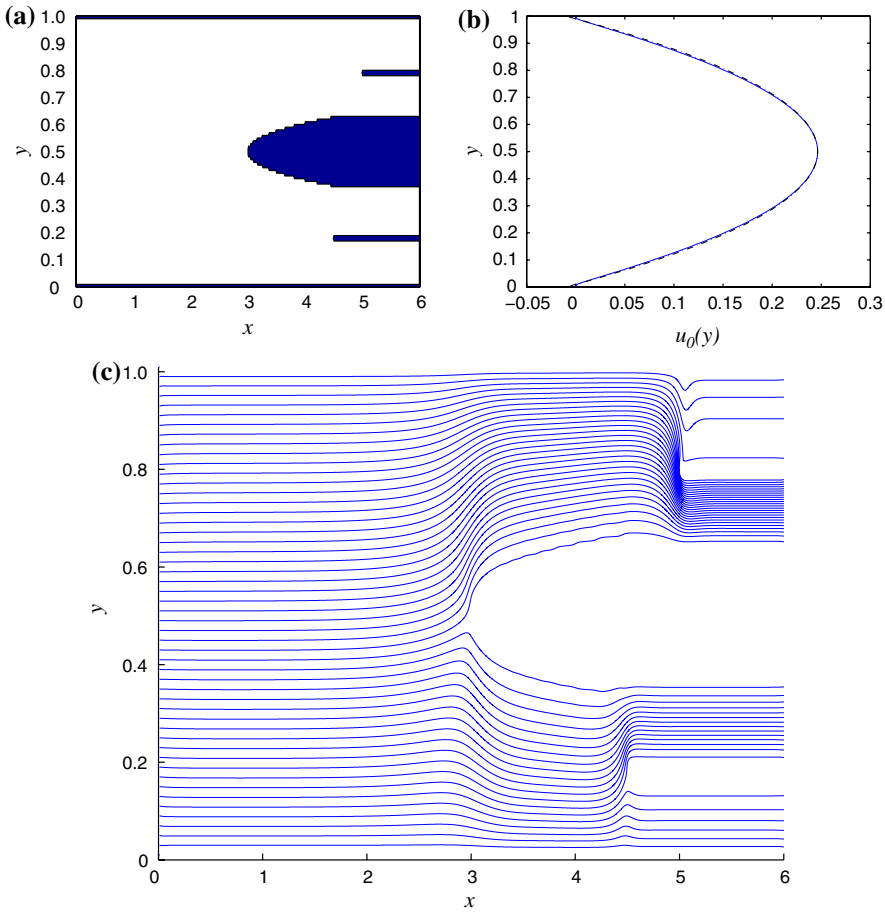

Fig. 13 Lattice-Boltzmann Simulation with 1-into-2-into-4 testcase with asymmetric end daughter pressures of values (from lower wall to upper wall) -0.75, -3.0, -7.5 and -0.75. (**a**) The geometrical setup showing the position of the dividers. (**b**) Nondimensional inlet profile $u(x = 0) = u_0(y)$ (solid) versus a Poiseuille profile (dotted). (**c**) Streamlines from LBM computation

Some results for the 1-into-2-into-4 case are presented in Figs. 13 and 14. Note that the incident velocity profile at $x = 0$ appears to be approximately Poiseuille again according to Fig. 13(b). As in the asymmetric single bifurcation channel in the previous subsection, there is strong evidence in Fig. 14(a–c) of upstream influence extending beyond an O(1) distance upstream of the central divider. However, notice that the upstream influence in the second generation of dividers, from daughter vessels to the four granddaughter vessels, exhibits severely abrupt pressure jumps only occurring within a very short distance ahead of the divider; this is fully in line with the predictions of the asymptotic theory given in Sect. 3. Examining more closely the upper and lower wall pressures and shear stresses in Fig. 14(a–c), one can observe that the initial free interaction upstream in the mother steers the majority of the flow into the upper daughter, leading to a fall in the lower wall shear stress; this recovers, however, as the central divider thickens downstream ahead of the second generation of dividers. In fact, curiously both daughter vessel flows become significantly attached on the outer walls upstream of the second generation of dividers where abrupt pressure jumps violently divert the flow into the more centrally positioned granddaughter vessels. This leads to a sudden adverse pressure gradient occurring at both upper and lower outer walls causing a sharp drop in wall shear stress and almost flow separation at the upper wall. Observe though that the flows in the outer granddaughters appear to rapidly recover within a small distance of the leading edges and revert to a Poiseuille like form which continues downstream to the edge of the computational domain.

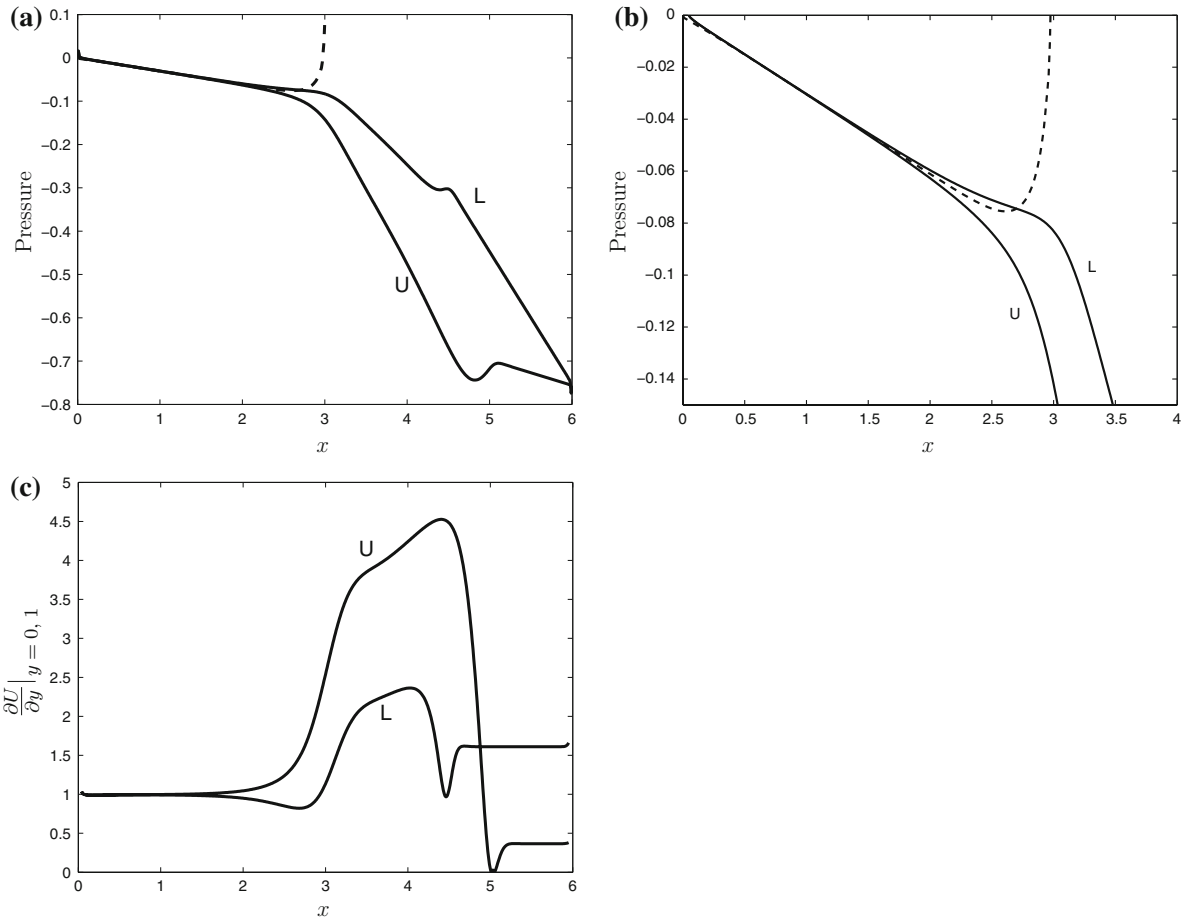

Fig. 14 Lattice-Boltzmann Simulation with 1-into-2-into-4 testcase with asymmetric end daughter pressures of values (from lower wall to upper wall) -0.75, -3.0, -7.5 and -0.75. (**a**) Nondimensional pressure at the lower wall (L) and upper wall (U) and on the midline $y = 0.5$ (dotted). (**b**) The same plot as (**a**) but focussing on the behaviour ahead of the central divider. (**c**) Nondimensional wall shear stress $\frac{\partial U}{\partial y}$ at the lower wall (L) and upper wall (U)

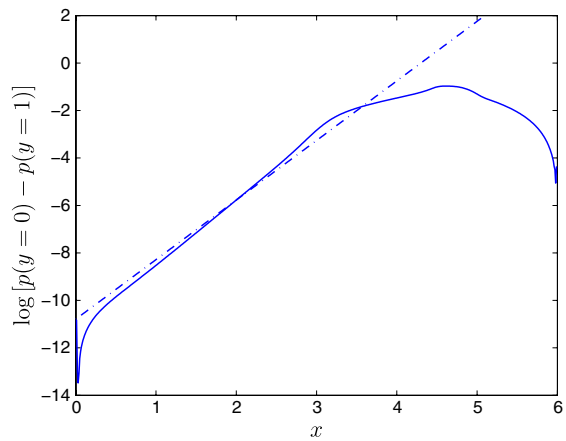

Fig. 15 LBM 1-into-2-into-4 case: Comparison of the log of the pressure difference between upper and lower walls obtained from the lattice-Boltzmann simulation (solid line) against our analytical theory which predicts a line of slope $\kappa \mathrm{Re}^{-1/7}$ (dotted line) upstream of the divider

A similar comparison to that for the asymmetric single bifurcation case above is shown in Fig. 15. Once again, κ is calculated by obtaining the values $q = 0.0313$ and $\lambda_0 = 1.0055$ from the incident velocity profile obtained in the lattice-Boltzmann simulation, and a straight line of the form (40) is drawn on the plot against the log of the pressure difference between the upper and lower walls. Once again, the agreement in the majority of the region upstream of the central divider is extremely good, with similar discrepancies as in the previous case existing between the computation and theory around $x = 0$ and near the start of the central divider that can be explained as above.

7 Further comments and conclusions

Non-symmetries due to the vessel shapes, end pressures or other factors can cause very significant non-symmetrical responses to propagate in the internal motion throughout the network of vessels, switching the overall flow from side to side by means of the displacement effect, and there is a correspondingly significant impact on the flow ahead of the network. The displacement response is much more pronounced in fact than that on the total mass flux in the current configurations since the induced displacement does not alter the total substantially. The results in the figures demonstrate that the upstream displacement can be to either side of the original mother vessel, depending on shapes as well as downstream pressures, and in addition the dependence is rather sensitive. The sensitivity is seen also in the formulae such as those at the end of Sect. 4 that involve integrated areas and pressure–momentum contributions supplied by all or part of the network. Although the bias due to non-symmetry is felt throughout the system, with widely differing mass-flux alterations inside internal vessels being given in effect by the $-\sigma$ terms in Sects. 3 and 4, the non-symmetric displacement effects are perhaps most keenly felt near the outer walls. The present typical network alters the distribution of the incident flux, in essence displacing some fluid that would otherwise go straight on axially into one or other side of the system.

Among other points stemming immediately from this study, the comparisons between the theory and direct simulations seem affirmative and highly encouraging. They tend to support the view that the flow displacement response in a large network is broadly but not entirely inviscid. Different types of bifurcation are involved and they need to communicate, requiring matching particularly via the pressure-jump phenomena occurring at the entrance to almost every vessel. In each inner vessel an inertial response is found in which conservation of mass and momentum yield increasing pressure when the gap width decreases, on a local basis, and this determines the mass flux in each such vessel. All such vessels are virtually independent, except that their end pressures are determined in an upstream-marching process and communication with neighbouring vessels takes place at each entrance as mentioned above. In each outer vessel of the system the core motion is parallel to the inner wall (a divider wall), although subject to an unknown uniform displacement in addition which usually depends on a large section of the network and that extra displacement itself is uniform only from one bifurcation to the next, i.e., is piecewise constant. The outer wall layers, however, are viscous and are controlled by the slip generated by the core coupled with the influence of the outermost wall shapes. Both the extreme and the linearized cases considered in this article suggest a rich structure and physics arising from the system. In addition, the combination of theoretical analysis and computations is encouraged.

Concerning nonlinear effects it would be of interest to see the network behaviour when the inner vessels exhibit nonlinear responses, bearing in mind that the first and the wall-touching branch junctions can be accompanied by nonlinear viscous wall layers, as is well known. The latter come into play when the outermost end-pressure differences are of opposite sign but differ in magnitude since then the free interaction upstream of the first branch junction has to be nonlinear. Moreover, end pressures in the outermost vessels comparable with those taken here for the inner vessels would almost certainly cause large-scale separation of a kind similar to that reported in [24,33], near the outermost walls.

Generalizations to allow for incident velocity profiles distinct from the fully developed forms studied here need hardly be repeated, and likewise for many other follow-on issues. It is worth remarking nonetheless that for a network containing vessels significantly longer than the present ones, specifically ones of non-dimensional length comparable with the Reynolds number, the incident-profile generalization certainly matters. As viscous effects fill

the typical vessel then, they produce new no-slip velocity profiles at the approach to each new bifurcation downstream, rather like the even longer-scale situation in the [20] network, except that non-symmetry causes the 1/7 free interaction of Sect. 2 to arise at every such bifurcation then, and this occurs even inside the internal units for example in contrast with the present configurations addressed in Sects. 3 and 4. A major goal, however, must be to accommodate three-dimensional networks. Indeed, common needs in virtually all network cases studied thus far are increased understanding of three-dimensional phenomena eventually and further investigation of full nonlinearity, as well as following through on ideas on wall flexibility, unsteadiness, and other continuing work. We aim to report more on three-dimensional branching effects later, concerning non-symmetry and upstream wall shaping. Regarding the biomedical applications mentioned early on in the paper, the presence of multiple jumps in the flow solutions is intriguing, for example with respect to the very high local pressure gradients and wall shear stresses thus induced at almost every vessel entrance in a network; branch junctions are known to be frequent sites of atherogenesis in general. The high gradients can be coupled with separation and eddies in nonlinear and/or unsteady cases; see in [22,23]. Finally here, various physical alterations to the network should be modelled, such as adding another incident feeding vessel (a second mother) to the whole system or cutting off some of the daughters, granddaughters and even an entire section of the network.

Acknowledgements We would like to thank EPSRC for support through the Mathematics Programme and Life Sciences interface, and also Neil Kitchen, Stefan Brew, Joan Grieve, Robert Bowles and Stephen Baigent and others in the UCL Medical Modelling Group for their interest and helpful discussions. The helpful comments and suggestions from the referees and the editor are gratefully acknowledged.

References

1. Pries AR, Secomb TW, Gaehtgens P (1998) Structural adaptation and stability of microvasular networks:theory and simulations. Am J Physiol Heart Circ Physiol 275:H349–H360
2. Hademenos GJ, Massoud TF, Viñuela F (1996) A biomathematical model of intracranial arteriovenous malformations based on electrical network analysis. Neurosurgery 38:1005–1015
3. Goldman D, Popel AS (2000) A computational study of the effect of capillary network anastomoses and tortuosity on oxygen transport. J Theor Biol 206(2):181–194
4. Brada M, Kitchen ND (2000) How effective is radiosurgery for arteriovenous malformations. J Neurol Neurosurg Psychiatry 68:548–549
5. McEvoy AW, Kitchen ND, Thomas DGT (2000) Intracerebral haemorrhage in young adults:the emergence of drug misuse. B Med J 320:1322–1324
6. Smith FT, Jones MA (2000) One-to-few and one-to-many branching tube flows. J Fluid Mech 423:1–31
7. Smith FT, Jones MA (2003) AVM Modelling by multi-branching tube flow:large flow rates and dual solutions. Math Med Biol 20:183–204
8. Young WL, Kader A, Pile-Spellman J, Ornstein E, Stein BM (1996) Arteriovenous malformation drawing vein physiology and determinants of transnidal pressure gradients. Neurosurgery 35:389–396
9. Gao E, Young WL, Pile-Spellman J, Joshi S, Duong H, Stieg PE, Ma Q (1997) Cerebral arteriovenous malformations feeding artery aneurysms:a theoretical model of intravascular pressure changes after treatment. Neurosurgery 41:1345–1358
10. Hademenos GJ, Massoud TF (1997) Biophysical mechanisms of stroke. Stroke 28:2067–2077
11. Zhao Y, Brunskill CT, Lieber BB (1997) Inspiratory and expiratory steady flow analysis in a model symmetrically bifurcating airway. J Biomech Eng 119(1):52–58
12. Wilquem F, Degrez G (1997) Numerical modelling of steady inspiratory airflow through a three-generation model of the human central airways. J Biomech Eng 119(1):59–65
13. Liu Y, So RM, Zhang CH (2003) Modeling the bifurcating flow in an asymmetric human lung airway. J Biomech 36(7):951–959
14. Kassab GS, Schatz A, Imoto K, Fung Y-C (2000) Remodeling of the bifurcation asymmetry of the right coronary ventricular branches in hypertrophy. Ann Biomed Eng 28(4):424–430
15. Lorthois S, Lagree P-Y, Marc-Vergnes J-P, Cassot F (2000) Maximal wall shear stress in arterial stenoses:application to the internal carotid arteries. J Biomech Eng 122(6):661–666
16. Comer JK, Kleinstreuer C, Zhang Z (2001) Flow structures and particle deposition patterns in double-bifurcation airway models. Part 1:air flow fields. J Fluid Mech 435:25–54
17. Cassidy KJ, Gavriely N, Grotberg JB (2001) Liquid plug flow in straight and bifurcating tubes. J Biomech Eng 123(6):580–589
18. Resnick N, Einav S, Chen-Konak L, Zilberman M, Yahav H, Shay-Salit A (2004) Haemodynamic forces as a stimulus for arteriogenesis. Endothelium 10:197–206
19. Alarcon T, Byrne HM, Maini PK (2005) A design principle for vascular beds:the effects of complex blood rheology. Microvascular Res 69:156–172

20. Bowles RI, Dennis SCR, Purvis R, Smith FT (2005) Multi-branching flows from one mother tube to many daughter or to a network. Phil Trans Roy Soc A 363:1045–1055
21. Tadjfar M, Smith FT (2004) Direct simulations and modelling of basic three-dimensional bifurcating tube flows. J Fluid Mech 519:1–32
22. Smith FT, Ovenden NC, Franke PT, Doorly DJ (2003) What happens to pressure when a flow enters a side branch. J Fluid Mech 479:231–258
23. Smith FT, Dennis SCR, Jones MA, Ovenden NC, Purvis R, Tadjfar M (2003) Fluid flows through various branching tubes. J Eng Maths 47:277–298
24. Smith FT (1977) Upstream interactions in channel flows. J Fluid Mech 79:631–655
25. Smith FT (1976) On entry-flow effects in bifurcating, blocked or constricted tubes. J Fluid Mech 78:709–736
26. Brotherton-Ratcliffe RV (1987) Boundary layer effects in liquid layer flows. Ph.D. Thesis, University of London
27. Chen S, Doolen GD (1998) Lattice Boltzmann method for fluid flows. Ann Rev Fluid Mech 30:329–364
28. Wolf-Gladrow DA (2000) Lattice-gas cellular automata and lattice Boltzmann models. Springer
29. Succi S (2001) The lattice Boltzmann equation for fluid dynamics and beyond. Oxford Science Publication
30. He X, Luo LS (1997) Lattice Boltzmann model for the incompressible Navier–Stokes equations. J Stat Phys 88(3/4):927
31. Bhatnagar P, Gross E, Krook M (1954) A model for collision processes in gases I:small amplitude processes in charged and neutral one-component system. Phys Rev 94:511
32. Zou Q, He X (1997) On pressure and velocity boundary conditions for the lattice Boltzmann BGK model. Phys Fluids 9:1591
33. Smith FT, Duck PW (1980) On the severe nonsymmetric constriction, curving and cornering of channel flows. J Fluid Mech 90: 727–753